ACCURATE VISIBLE LIGHT POSITIONING THROUGH POWER ADAPTATION OF LED ARRAYS

A THESIS SUBMITTED TO

THE GRADUATE SCHOOL OF ENGINEERING AND SCIENCE

OF BILKENT UNIVERSITY

IN PARTIAL FULFILLMENT OF THE REQUIREMENTS FOR

THE DEGREE OF

MASTER OF SCIENCE

IN

ELECTRICAL AND ELECTRONICS ENGINEERING

By

Ramazan YAZ

August 2025

Accurate Visible Light Positioning through Power Adaptation of LED Arrays
By Ramazan YAZ
August 2025

We certify that we have read this thesis and that in our opinion it is fully adequate, in scope and in quality, as a thesis for the degree of Master of Science.

Sinan Gezici (Advisor)

Tolga Mete Duman

Berkan Dülek

Approved for the Graduate School of Engineering and Science:

Orhan Arıkan
Director of the Graduate School

ABSTRACT

ACCURATE VISIBLE LIGHT POSITIONING THROUGH POWER ADAPTATION OF LED ARRAYS

Ramazan YAZ
M.S. in Electrical and Electronics Engineering
Advisor: Sinan Gezici
August 2025

In this thesis, we develop power allocation strategies for asynchronous visible light positioning (VLP) systems employing light-emitting diode (LED) arrays with the aim of improving localization accuracy. We first review the literature on visible light positioning in indoor scenarios. Then, we formulate an optimization problem for minimizing the Cramér-Rao lower bound (CRLB) related to the estimation of the receiver location subject to practical constraints on total and individual transmission powers and required illumination levels. Due to the non-convexity of the proposed formulation, we devise a two-step methodology. First, a convex optimization problem is employed to determine the power allocation that maximizes the total received power. Subsequently, a projected gradient descent algorithm is utilized to refine the power allocation according to the CRLB metric under the power and illumination constraints. In addition, a framework for iterative power allocation and localization is developed for practical deployment, in which each step of the optimization process uses the most recent position estimate. Simulation results indicate that the proposed method can outperform both the uniform and power maximization based allocation schemes, resulting in improved localization accuracy over a wide range of operating conditions. Hence, it can provide robust and high-precision indoor positioning, even in circumstances involving asynchronous transmission and stringent illumination requirements.

Keywords: Visible light positioning (VLP), light emitting diode (LED), estimation, localization, Cramér-Rao lower bound (CRLB).

ÖZET

LED DİZİLERİNDE GÜÇ UYARLAMASI İLE HASSAS GÖRÜNÜR IŞIK KONUMLANDIRMA

Ramazan YAZ
Elektrik ve Elektronik Mühendisliği, Yüksek Lisans
Tez Danışmanı: Sinan Gezici
Ağustos 2025

Bu tezde, konumlandırma doğruluğunu iyileştirme amacıyla ışık yayan diyot dizileri kullanan asenkron görünür ışık konumlandırma sistemleri için güç tahsis stratejileri geliştirmekteyiz. İlk olarak iç mekan senaryolarında görünür ışık konumlandırması ile ilgili literatürü incelemekteyiz. Ardından, alıcı konumunun kestirimiyle ilişkili Cramér-Rao alt sınırını (CRAS) en aza indirmeyi amaçlayan bir optimizasyon problemini, toplam ve bireysel iletim güçleri ile gerekli aydınlatma düzeylerine ilişkin pratik kısıtlar altında formüle etmekteyiz. Önerilen formülasyonun dışbükey bir yapıda olmaması nedeniyle, iki adımlı bir metodoloji tasarlamaktayız. İlk olarak, toplam alınan gücü en üst düzeye çıkaran güç dağılımını belirlemek için dışbükey bir optimizasyon problemi kullanılmaktadır. Bunu takiben, güç ve aydınlatma kısıtlamaları altında CRAS metriğine göre güç tahsisini iyileştirmek için projeksiyonlu gradyan iniş algoritması kullanılmaktadır. Ayrıca, pratik uygulamalar için her optimizasyon adımında en güncel konum kestiriminin kullanıldığı yinelemeli güç tahsisi ve konumlandırma sistemi geliştirilmiştir. Simülasyon sonuçları önerilen yöntemin hem eşit tahsis hem de güç maksimizasyonuna dayalı tahsis yaklaşımlarından daha iyi performans gösterebildiğini ve geniş çalışma koşulları aralığında konumlandırma doğruluğunu artırdığını göstermektedir. Dolayısıyla, önerilen yöntem asenkron iletim ve sıkı aydınlatma gereksinimlerinin söz konusu olduğu durumlarda dahi gürbüz ve yüksek hassasiyetli iç mekan konumlandırması sağlayabilmektedir.

Anahtar sözcükler: Görünür ışık konumlandırma, ışık yayan diyot, kestirim, konumlandırma, Cramér-Rao alt sınırı.

Acknowledgement

First of all, I am deeply grateful to my advisor, Prof. Sinan Gezici. I am sincerely thankful for his support, understanding, patience, and kindness throughout my education at Bilkent. He was always available and communicated exceptionally well with me. I feel extremely blessed to have him as an advisor during my graduate studies, and to receive his guidance. I can't express the respect and admiration I have for him as a knowledgeable scholar and a humble mentor. It was a privilege and an honor to work with you, thank you hocam!

Secondly, I would like to thank Prof. Tolga Mete Duman and Prof. Berkan Dülek for agreeing to serve on my thesis defense committee and for their time and contributions.

I also wish to express my special thanks to Türk Telekom A.Ş. for supporting my research throughout the program.

I am also thankful to my friends Emir, İsmail Mert, Fatih, Mahmut, İsmail Enes, Issifu, as well as all the others whose names I cannot mention. Thank you for being there for me in my good and bad days. Your support was invaluable. I consider each one of you as a brother.

Finally, I would like to express my gratitude to my family. I cannot thank my mom enough. No words can express how grateful I am to her for her love, endless support, and encouragement. My dad is a great father who is like an invincible mountain standing behind me, supporting. Thank you both for the sacrifices you made for me. I hope I have made you proud. I would like to thank my brothers for putting up with me and tolerating me even though they can be justifiably annoying at times. I know I am not easy, sorry about that.

Contents

List of Figures

List of Tables

Chapter 1

Introduction

1.1 Literature Review

Indoor localization has become a fundamental facilitator for developing location-based services within building infrastructure [1, 2]. In indoor environments, the reliability of satellite signals is significantly compromised in comparison to outdoor environments, where global navigation satellite systems (GNSS) are typically more effective [3]. This discrepancy can be attributed to the fact that radio propagation in such environments is characterised by a series of complex phenomena, including attenuation, reflection, diffraction, and multipath, which significantly impede signal transmission and reception. Therefore, there is a necessity for the implementation of dedicated techniques, taxonomies and evaluation metrics tailored to indoor environments in order to successfully execute tasks related to localization [1–5]. The potential application areas of such tasks are extensive, ranging from healthcare facilities (real-time location systems for patient/asset flow and safety), advanced industrial environments and logistics (resource tracking and human–robot coordination), public venues (wayfinding and occupancy analytics), retail (in-store analytics), and augmented reality (AR)/virtual reality (VR) experiences that depend on precise, low-latency pose or position estimates [4–8].

Radio frequency (RF) based indoor positioning systems have been the subject of considerable academic research in the field of indoor localization [1, 2, 4, 9]. These systems have evolved around a variety of radio technologies such as Wi-Fi, bluetooth low energy beacons, ultra-wideband (UWB), RFID, and cellular due to their pervasive use and cost-effectiveness [10–14]. In spite of the consistent progress and considerable research that has been conducted over the course of several decades, practical implementations continue to encounter limitations that have been outlined in the literature. These limitations can be categorised as follows: multipath sensitivity, calibration burden, shared-spectrum interference/congestion and in certain contexts (e.g. hospitals/aircraft), electromagnetic compatibility concerns [4, 12–16]. Consequently, a system that is cost-effective, accurate and universally accessible does not yet exists. For instance, although UWB can achieve high accuracy, it generally comes with higher device cost and energy consumption, requires precise anchor synchronization, and exhibits performance degradation in severe non-line-of-sight (NLOS) conditions, thereby hindering its universal adoption in large public spaces [14, 17]. As a result, visible light positioning (VLP) has gained considerable attention as a promising alternative to RF based localization, particularly in indoor environments [18–21]. Leveraging light emitting diodes (LEDs) as both illumination sources and positioning anchors, VLP systems provide precise localization by utilizing received optical signals from LED transmitters at known locations [21, 22]. Unlike RF based positioning, VLP benefits from unlicensed spectrum, reduced interference, and specific line-of-sight (LOS) properties of visible light. Additionally, VLP systems exploit existing LED infrastructures, leading to reduced deployment costs and energy consumption [23].

A considerable number of applications and location-based services have been developed that incorporate VLP systems. The ubiquity and controllability of LED light fixtures make VLP a suitable solution for high-resolution indoor wayfinding in large public venues, such as airports, shopping malls, and museums [18]. In such environments, the ability to ensure accuracy and low latency at either the aisle- or metre-level is crucial for effective pedestrian navigation and accessibility services. In the field of healthcare, VLP facilitates precise tracking of both equipment and patients as well as monitoring the location of a mobile medical device or a wheelchair [16, 18]. The deployment of VLP systems in industrial and logistics settings facilitates the localization of assets, ensures work-in-process visibility, and provides guidance for autonomous mobile robots operating within dense spatial reuse environments to maintain continuity in occlusions [24, 25] . Moreover, the compact spatial confinement and elevated data density of light attocells make VLP systems a compelling solution for room-scale AR/VR pose anchoring and hybrid light fidelity (LiFi)/VLP services that leverage existing lighting infrastructure. In summary, VLP is a suitable choice for applications in smart environments, industrial automation, and intelligent transportation systems [16, 26].

For a given VLP system, theoretical limits on position estimation accuracy and optimal estimators that (asymptotically) achieve those limits have been studied in numerous studies in the literature such as [27–38]. In [27], both received signal strength (RSS) and angle-of-arrival (AOA) measurements are employed within a visible light communication (VLC) system with multiple LED transmitters and a single receiver for three-dimensional (3D) localization. The study also derives the Cramér-Rao lower bound (CRLB) based on RSS, specifying 3D positioning performance across various deployment scenarios. Similarly, RSS and AOA are utilized in a 3D indoor positioning method involving a single LED array and multiple VLC receivers in [28]. The time differences of arrival (TDOA) of the pilot signals received from LED panels located on the ceiling are utilized to estimate the position of the receiver in [29]. Two-dimensional VLP based on RSS is explored in [32] and [33], assuming a fixed receiver height. This setup employs an aperture-based receiver, and the CRLB is derived to assess the effectiveness of the proposed positioning algorithms. Moreover, [35] analyzes the influence of non-line-of-sight (NLOS) components, signal-to-noise ratio (SNR), transmission distance, and the number of LED sources on the performance of RSS-based VLP systems, providing closed-form CRLB expressions for both position and orientation estimation. In [37], CRLBs and maximum likelihood (ML) estimators are derived for both synchronous and asynchronous VLP networks considering direct and two-step positioning approaches. It is shown that the two-step approach is equivalent to the direct ML estimator for asynchronous VLP systems. In addition, the work in [38] investigates joint position and orientation estimation in RSS-based VLP systems using multiple LED transmitters and multiple VLC receivers.

A noteworthy volume of research has been conducted in the literature on the utilization of machine learning approaches in VLP systems in conjunction with the methods based on visible light propagation models [39–57]. Learning-based VLP involves the process of determining the location of an object or a subject in relation to its surrounding environment through the use of data-driven methodologies such as regression methods, deep artificial neural networks (ANN), convolutional neural networks (CNN), k-nearest neighbors (k-NN), support vector machines (SVM), etc. [49–57]. These approaches involve the conversion of optical features, such as received signal strength (RSS), power spectral features, or channel state, measured by photodiodes, or image features captured by cameras, into two-dimensional (2D)/three-dimensional (3D) coordinates. Nevertheless, the aforementioned methods are subject to certain practical drawbacks, motivating the development of model-based (or hybrid) alternatives. They are data-hungry, which can incur significant costs, require substantial labour, and may not be suitable for all applications. Moreover, these methods are environment-specific, often resulting in failure to generalize across buildings or the necessity of frequent recalibration and relabelling [57]. Consequently, this thesis focuses on a model-based VLP approach.

Once optimal estimators are designed for VLP systems as in [37, 38], further improvements on localization accuracy can be achieved by optimizing the parameters of LED transmitters. In particular, a key challenge in VLP systems is to optimize the transmission parameters of LEDs to enhance localization accuracy while considering practical system constraints such as power limitations and illumination requirements. Previous research has focused on power allocation strategies for LED transmitters to minimize localization errors by optimizing the CRLB, thereby improving positioning performance under various uncertainty models [58–64]. Specifically, [59] proposes an optimal and robust power allocation framework for LED transmitters to minimize the localization error of VLC receivers while satisfying practical power and illumination constraints. This approach demonstrates significant improvements over uniform power allocation strategies by leveraging convex optimization and robust design principles. In [61], a robust power allocation scheme is introduced that jointly optimizes positioning accuracy and data throughput under random positioning errors. By formulating a chance-constrained optimization problem and deriving explicit relationships between positioning and channel state information uncertainties, the authors transform these probabilistic constraints into convex forms. The proposed approach yields superior localization performance and communication reliability in comparison with conventional uniform or non-robust allocation strategies. On the other hand, [62] introduces a power-efficient positioning framework for VLC networks by formulating a chance-constrained optimization problem to minimize the total transmit power of LED arrays while guaranteeing that the CRLB on localization errors remains below a desired threshold with high probability. This approach accounts for stochastic uncertainties in system parameters by imposing probabilistic (rather than deterministic) constraints on localization accuracy and enables robust performance improvements over both non-robust methods and uniform power allocation strategies.

1.2 Contributions

Although power allocation problems have been investigated for VLP systems in the literature such as [59, 61, 64], there exist no studies that investigate optimal power allocation for *LED arrays* in asynchronous VLP systems for minimizing the CRLB under power and illumination constraints. In this thesis, we develop a new power allocation technique for LED arrays in asynchronous VLP systems, which effectively performs spatial beamforming for improving localization accuracy by jointly optimizing the power distribution among multiple LEDs within each array [65] . After formulating the proposed problem of power allocation for LED arrays under practical power and illumination constraints, we solve it in two steps. We first find an initial solution, which is obtained by solving a convex problem corresponding to received power maximization. Then, we employ a projected gradient descent algorithm starting from that initial solution by utilizing an explicit expression for the gradient term. In addition, we develop an iterative version of the algorithm for practical scenarios where power allocation and localization are performed iteratively.

The main contributions and novelty of this thesis are summarized as follows:

- We propose a power allocation (effectively, beamforming) approach for LED arrays in an asynchronous VLP system to minimize the CRLB on position estimation under practical power and illumination constraints.

- We derive a CRLB expression for position estimation in terms of transmit power parameters of LED arrays, which is a non-convex function in general (unlike the convex CRLB expression in [59] derived for transmitters with single LEDs).

- To obtain a solution of the non-convex problem of power allocation, we first focus on the problem of received power maximization, which results in a convex problem and provides an initial point for the proposed non-convex optimization problem. Then, we explicitly calculate the gradient of the CRLB and minimize it under the power and illumination constraints via projected gradient descent.

- For practical deployments, we propose an iterative approach of power allocation and localization, where the VLC receiver performs ML based localization and the power allocation is performed based on the ML estimates.

Via simulation results, we demonstrate the effectiveness of our proposed power allocation strategy in improving localization performance compared to conventional uniform power allocation and received power maximization techniques.

1.3 Organization of the Thesis

The organization of this thesis is described as follows. In Chapter 2, the problem of power allocation for LED arrays in asynchronous VLP systems under practical power and illumination constraints is formulated, and two algorithms are proposed to tackle this problem. In Chapter 3, simulation results are presented and the performances of the proposed algorithms are analyzed. The concluding remarks and proposed future research are addressed in Chapter 4.

Chapter 2

Power Allocation for LED Arrays

In this chapter, we investigate optimal power allocation for LED arrays in asynchronous VLP systems for minimizing the CRLB under power and illumination constraints. We begin by presenting the system model upon which we base our work. Subsequently, the derivation of the CRLB for the specified configuration is provided. Then, we proceed to illustrate the power and illumination constraints and formulate an optimization problem for minimizing the CRLB subject to these constraints. Finally, we propose our methods addressing this optimization problem.

2.1 System Model

We focus on a VLP system with N LED arrays, where the ith LED array consist of L_i LEDs for $i = 1, \ldots, N$. The location and the orientation vector of the jth LED in the ith LED array are denoted by $\boldsymbol{l}_{i,j}$ and $\boldsymbol{n}_{i,j}$, respectively, which are assumed to be known for all $j \in \{1, \ldots, L_i\}$ and $i \in \{1, \ldots, N\}$. We consider the localization of a generic VLC receiver at an unknown location denoted by $\boldsymbol{x}$, and assume that the VLC receiver knows its orientation vector denoted by $\bar{\boldsymbol{n}}$, which can be determined, for example, via a gyroscope [59, 66].

Considering an asynchronous VLP system, in which the VLC receiver is not synchronized with the LED arrays [37], the aim is for the VLC receiver to estimate its unknown location $\boldsymbol{x}$ based on power measurements of incoming signals emitted by the LED arrays. We propose a system in which the LEDs in each LED array transmit the scaled version of a base signal simultaneously during each localization interval. More specifically,

$$s_{i,j}(t) = \sqrt{w_{i,j}}\,\tilde{s}_i(t) \tag{2.1}$$

represents the transmitted optical signal from the jth LED in the ith LED array, where $w_{i,j} \geq 0$ is the transmit power parameter and $\tilde{s}_i(t)$ denotes a base signal for the ith LED array, which satisfies $\int_0^{T_{\mathrm{s},i}} \tilde{s}_i^2(t)dt/T_{\mathrm{s},i} = 1$ with $[0, T_{\mathrm{s},i}]$ representing the interval for the support of $\tilde{s}_i$ for $i = 1, \ldots, N$. The block diagram for an LED array is shown in Fig. 2.1.

Assuming a certain type of multiplexing approach, e.g., frequency or code division multiplexing, the VLC receiver observes the signals coming from the LED arrays separately [67,68]. Also, as in [30,37,38,69,70], only the LOS signals between the LEDs and the VLC receiver are considered. Accordingly, the signal received at the VLC receiver due to the signals from the ith LED array can be modeled as follows:

$$r_i(t) = R_p \sum_{j=1}^{L_i} h_{i,j}\sqrt{w_{i,j}}\,\tilde{s}_i(t-\tau_{i,j}) + \tilde{\eta}_i(t) \tag{2.2}$$

for $i \in \{1, \ldots, N\}$ and $t \in [T_{1,i}, T_{2,i}]$, where $T_{1,i}$ and $T_{2,i}$ specify the observation interval for the signal coming from the ith LED array, R_p is the responsivity of the photo-detector at the VLC receiver, $h_{i,j}$ is the channel gain of the signal between the jth LED in the ith LED array and the VLC receiver, $\tau_{i,j}$ is the time-of-arrival of the signal emitted by jth LED in the ith LED array, and $\tilde{\eta}_i(t)$ is zero-mean white Gaussian noise with a spectral density level of σ^2.

Considering practical indoor environments and LED array sizes, the duration of the optical signals in (2.1) is commonly much longer than the differences among the TOA's of the incoming signals from a given LED array; namely, among $\tau_{i,1}, \ldots, \tau_{i,L_i}$. Therefore, $\tilde{s}_i(t-\tau_{i,j}) \approx \tilde{s}_i(t-\tau_i)$ for $j = 1, \ldots, L_i$ for each

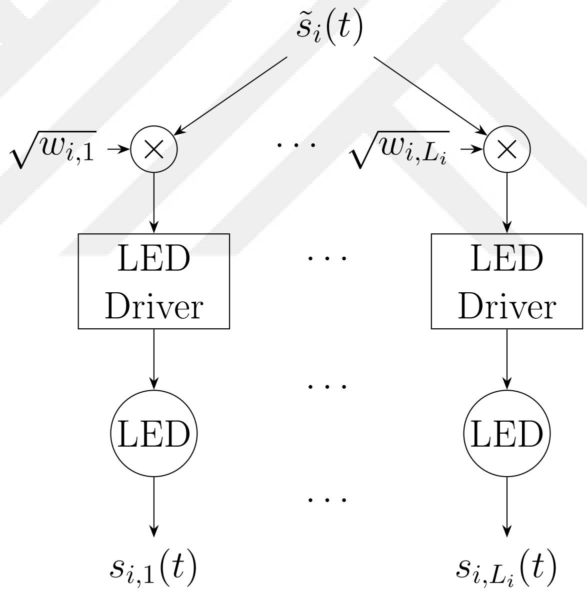

Figure 2.1: The block diagram of the ith LED array in the considered VLP system, where $i \in \{1, \ldots, N\}$.

$i \in \{1, \ldots, N\}$, where τ_i can be set to one of $\tau_{i,1}, \ldots, \tau_{i,L_i}$. Accordingly, (2.2) can be stated as

$$r_i(t) = R_p \left(\sum_{j=1}^{L_i} h_{i,j} \sqrt{w_{i,j}} \right) \tilde{s}_i(t - \tau_i) + \tilde{\eta}_i(t) \tag{2.3}$$

Since τ_i's are unknown in asynchronous VLP systems, the power of the received signal in (2.3) can be obtained by correlating it with $\tilde{s}_i(t - \tau)$ for all possible τ values and determining the peak value, as described in [37]. Consequently, the received power measurement at the VLC receiver due to the signal from the ith LED array can be modeled as follows (after some normalization to remove the constant terms for simplifying the notation) [31, 66, 71, 72]:

$$P_{\mathrm{RX},i} = \sum_{j=1}^{L_i} h_{i,j} \sqrt{w_{i,j}} + \eta_i \,, \quad i = 1, \ldots, N \tag{2.4}$$

where η_i is a zero-mean Gaussian noise component with a variance of σ_i^2, which is independent of η_j for all $j \neq i$ [72].

The channel gain $h_{i,j}$ in (2.4) can be expressed as

$$h_{i,j} = \frac{(m_{i,j} + 1) A \left(\cos \phi_{i,j} \right)^{m_{i,j}} T_s(\psi_{i,j}) g(\psi_{i,j}) \cos \psi_{i,j}}{2\pi \| \boldsymbol{x} - \boldsymbol{l}_{i,j} \|^2} \tag{2.5}$$

where $m_{i,j}$ is the Lambertian order for the jth LED in the ith LED array, A is the area of the photo-detector at the VLC receiver, $\phi_{i,j}$ and $\psi_{i,j}$ are, respectively, the irradiance angle and the incidence angle for the LOS path between the jth LED in the ith LED array and the VLC receiver, and $T_s(\psi)$ and $g(\psi)$ are, respectively, the optical filter gain and the optical concentrator gain at the VLC receiver [71]. It is common to have a design with $T_s(\psi) g(\psi)$ being a constant [71]; hence, it can be set to unity to simplify the notation. Although the preceding expressions are presented as if all the LEDs are in the field-of-view (FOV) of the photo-detector at the VLC receiver, these formulations can still be used if some LEDs are not in the FOV of the photo-detector by excluding those LEDs from the CRLB expressions in Section 2.2. (Commonly, the LED transmitters are at the ceiling of a room, and the VLC receiver is close to the floor level pointing upwards and having a

FOV of 90^o by using a hemispherical lens [73, 74]. Hence, most of the LEDs are in the FOV of the VLC receiver in practical applications.)

By calculating the angles in (2.5) based on the geometric relations of $(\boldsymbol{x} - \boldsymbol{l}_{i,j})^T \boldsymbol{n}_{i,j} = \|\boldsymbol{x} - \boldsymbol{l}_{i,j}\| \cos\phi_{i,j}$ and $(\boldsymbol{l}_{i,j} - \boldsymbol{x})^T \bar{\boldsymbol{n}} = \|\boldsymbol{l}_{i,j} - \boldsymbol{x}\| \cos\psi_{i,j}$, the channel gain in (2.5) can be expressed as follows:

$$h_{i,j} = \frac{(m_{i,j}+1)A\left((\boldsymbol{x} - \boldsymbol{l}_{i,j})^T \boldsymbol{n}_{i,j}\right)^{m_{i,j}} (\boldsymbol{l}_{i,j} - \boldsymbol{x})^T \bar{\boldsymbol{n}}}{2\pi \|\boldsymbol{x} - \boldsymbol{l}_{i,j}\|^{m_{i,j}+3}}. \tag{2.6}$$

By adjusting the transmit power parameters $w_{i,j}$ in (2.4), the LED arrays can effectively form beams in specific directions. The aim is to design these power parameters of the LEDs in each LED array for enhancing the localization accuracy. Since the design for a specific position estimator would not be practical, we consider a theoretical performance metric based on the Fisher information matrix (FIM) related to estimating the position of the VLC receiver. Such approaches have been used in the literature extensively due to their practicality, generality, and asymptotic relation to ML estimation [75]. In this manuscript, we consider the minimization of the trace of the inverse FIM, i.e., CRLB, which provides a lower limit on mean squared errors (MSEs) of unbiased estimators. It is known that the MSE of the ML estimator converges to the CRLB in the high SNR regime [76].

2.2 Derivation of CRLB

To derive the CRLB for the proposed setting, we first consider the received power model given in (2.4) and obtain the log-likelihood function for the unknown position $\boldsymbol{x}$ based on the received power vector $\boldsymbol{P}_{\rm RX} = [P_{{\rm RX},1} \ldots P_{{\rm RX},N}]^T$ (i.e., the logarithm of the conditional probability density function of $\boldsymbol{P}_{\rm RX}$ given $\boldsymbol{x}$) as [76]

$$\Lambda(\boldsymbol{x}) = \tilde{k} - \sum_{i=1}^{N} \frac{1}{2\sigma_i^2} \left(P_{{\rm RX},i} - \sum_{j=1}^{L_i} h_{i,j}\sqrt{w_{i,j}}\right)^2 \tag{2.7}$$

where $\tilde{k}$ is a normalizing constant that does not depend on the unknown parameter vector $\boldsymbol{x}$.

The CRLB on the variance of any unbiased estimator $\hat{\boldsymbol{x}}$ for the location of the VLC receiver $\boldsymbol{x}$ can be expressed as [76]

$$\mathbb{E}\left\{||\hat{\boldsymbol{x}}-\boldsymbol{x}||^2\right\} \leq \text{trace}\left\{\mathbf{J}^{-1}(\boldsymbol{x})\right\} \tag{2.8}$$

where $\mathbf{J}(\boldsymbol{x})$ is the FIM for $\boldsymbol{x}$, which is defined as

$$\mathbf{J}(\boldsymbol{x}) = \mathbb{E}\left\{\left(\nabla_{\boldsymbol{x}}\Lambda(\boldsymbol{x})\right)\left(\nabla_{\boldsymbol{x}}\Lambda(\boldsymbol{x})\right)^T\right\}. \tag{2.9}$$

In (2.9), $\nabla_{\boldsymbol{x}}\Lambda(\boldsymbol{x})$ represents the gradient of $\Lambda(\boldsymbol{x})$ in (2.7) with respect to $\boldsymbol{x} = [x_1\ x_2\ x_3]^T$. The elements of the FIM in (2.9) can be expressed as

$$[\mathbf{J}(\boldsymbol{x})]_{k_1,k_2} = \mathbb{E}\left\{\frac{\partial\Lambda(\boldsymbol{x})}{\partial x_{k_1}}\frac{\partial\Lambda(\boldsymbol{x})}{\partial x_{k_2}}\right\} \tag{2.10}$$

for $k_1, k_2 \in \{1, 2, 3\}$, which can be calculated based on (2.7) as follows:

$$[\mathbf{J}(\boldsymbol{x})]_{k_1,k_2} = \sum_{i=1}^{N}\frac{1}{\sigma_i^2}\left(\sum_{j=1}^{L_i}\sqrt{w_{i,j}}\frac{\partial h_{i,j}}{\partial x_{k_1}}\right)\left(\sum_{j=1}^{L_i}\sqrt{w_{i,j}}\frac{\partial h_{i,j}}{\partial x_{k_2}}\right) \tag{2.11}$$

In (2.11), the partial derivatives are given by [66]

$$\begin{aligned}\frac{\partial h_{i,j}}{\partial x_k} = \frac{-(m_{i,j}+1)A}{2\pi\|\boldsymbol{x}-\boldsymbol{l}_{i,j}\|^{m_{i,j}+3}}\Bigg[&\bar{n}_k\left((\boldsymbol{x}-\boldsymbol{l}_{i,j})^T\boldsymbol{n}_{i,j}\right)^{m_{i,j}} \\ &- m_{i,j}n_{i,j,k}\left((\boldsymbol{x}-\boldsymbol{l}_{i,j})^T\boldsymbol{n}_{i,j}\right)^{m_{i,j}-1}(\boldsymbol{l}_{i,j}-\boldsymbol{x})^T\bar{\boldsymbol{n}} \\ &+ \frac{(m_{i,j}+3)(x_k-l_{i,j,k})\left((\boldsymbol{x}-\boldsymbol{l}_{i,j})^T\boldsymbol{n}_{i,j}\right)^{m_{i,j}}(\boldsymbol{l}_{i,j}-\boldsymbol{x})^T\bar{\boldsymbol{n}}}{\|\boldsymbol{x}-\boldsymbol{l}_{i,j}\|^2}\Bigg]\end{aligned} \tag{2.12}$$

where $\bar{n}_k$, $n_{i,j,k}$, and $l_{i,j,k}$ denote the kth elements of $\bar{\boldsymbol{n}}$, $\boldsymbol{n}_{i,j}$, and $\boldsymbol{l}_{i,j}$, respectively.

By defining $\sqrt{\boldsymbol{w}_i} \triangleq \left[\sqrt{w_{i,1}}\cdots\sqrt{w_{i,L_i}}\right]^T$ as the vector of transmit power parameters for the ith LED array and $\boldsymbol{h}_i = [h_{i,1}\cdots h_{i,L_i}]^T$ as the channel gain vector related to the LEDs in the ith LED array and the VLC receiver, we can state (2.11) as follows:

$$[\mathbf{J}(\boldsymbol{x})]_{k_1,k_2} = \sum_{i=1}^{N}\frac{1}{\sigma_i^2}\sqrt{\boldsymbol{w}_i}^T\left(\frac{\partial\boldsymbol{h}_i}{\partial\boldsymbol{x}_{k_1}}\frac{\partial\boldsymbol{h}_i^T}{\partial\boldsymbol{x}_{k_2}}\right)\sqrt{\boldsymbol{w}_i}\,. \tag{2.13}$$

The expression in (2.13) can be written as

$$[\mathbf{J}(\boldsymbol{x})]_{k_1,k_2} = \sum_{i=1}^{N}\sqrt{\boldsymbol{w}_i}^T\boldsymbol{H}^i_{k_1,k_2}\sqrt{\boldsymbol{w}_i} \tag{2.14}$$

where $\boldsymbol{H}^i_{k_1,k_2} \triangleq \frac{1}{\sigma_i^2}\left(\frac{\partial \boldsymbol{h}_i}{\partial \boldsymbol{x}_{k_1}}\frac{\partial \boldsymbol{h}_i^T}{\partial \boldsymbol{x}_{k_2}}\right)$. As a result, we can obtain the FIM as

$$\mathbf{J}(\boldsymbol{x}) = \begin{bmatrix} \sqrt{\boldsymbol{w}}^T \boldsymbol{H}_{1,1}\sqrt{\boldsymbol{w}} & \sqrt{\boldsymbol{w}}^T \boldsymbol{H}_{1,2}\sqrt{\boldsymbol{w}} & \sqrt{\boldsymbol{w}}^T \boldsymbol{H}_{1,3}\sqrt{\boldsymbol{w}} \\ \sqrt{\boldsymbol{w}}^T \boldsymbol{H}_{2,1}\sqrt{\boldsymbol{w}} & \sqrt{\boldsymbol{w}}^T \boldsymbol{H}_{2,2}\sqrt{\boldsymbol{w}} & \sqrt{\boldsymbol{w}}^T \boldsymbol{H}_{2,3}\sqrt{\boldsymbol{w}} \\ \sqrt{\boldsymbol{w}}^T \boldsymbol{H}_{3,1}\sqrt{\boldsymbol{w}} & \sqrt{\boldsymbol{w}}^T \boldsymbol{H}_{3,2}\sqrt{\boldsymbol{w}} & \sqrt{\boldsymbol{w}}^T \boldsymbol{H}_{3,3}\sqrt{\boldsymbol{w}} \end{bmatrix} \tag{2.15}$$

where $\sqrt{\boldsymbol{w}} \triangleq \left[\sqrt{\boldsymbol{w}_1}^T \ldots \sqrt{\boldsymbol{w}_N}^T\right]^T$ and $\boldsymbol{H}_{k_1,k_2}$ is given by

$$\boldsymbol{H}_{k_1,k_2} = \mathrm{blkdiag}\left(\boldsymbol{H}^1_{k_1,k_2}, \ldots, \boldsymbol{H}^N_{k_1,k_2}\right) \tag{2.16}$$

That is, $\boldsymbol{H}_{k_1,k_2}$ is a block diagonal matrix whose blocks are $\boldsymbol{H}^i_{k_1,k_2}$ for $i = 1, \ldots, N$.

The FIM given in (2.15) can be written in a compact form as

$$\mathbf{J}(\boldsymbol{x}) = \left(\mathbf{I}_3 \otimes \sqrt{\boldsymbol{w}}\right)^T \boldsymbol{H} \left(\mathbf{I}_3 \otimes \sqrt{\boldsymbol{w}}\right) \tag{2.17}$$

where $\mathbf{I}_3$ is the 3×3 identity matrix, $\otimes$ represents the Kronecker product, and $\boldsymbol{H}$ is a block matrix whose blocks are the $\boldsymbol{H}_{k_1,k_2}$ matrices; i.e.,

$$\boldsymbol{H} = \begin{bmatrix} \boldsymbol{H}_{1,1} & \boldsymbol{H}_{1,2} & \boldsymbol{H}_{1,3} \\ \boldsymbol{H}_{2,1} & \boldsymbol{H}_{2,2} & \boldsymbol{H}_{2,3} \\ \boldsymbol{H}_{3,1} & \boldsymbol{H}_{3,2} & \boldsymbol{H}_{3,3} \end{bmatrix}. \tag{2.18}$$

The aim is to minimize the CRLB in (2.17) subject to practical power and illumination constraints, which are described next.

2.3 Power Constraints

For LEDs to operate in the linear region and to achieve efficient electrical to optical conversion, lower and upper limits can be imposed on the transmit powers [59]. Accordingly, the transmit power parameters are constrained as

$$w^{\mathrm{low}}_{i,j} \leq w_{i,j} \leq w^{\mathrm{upp}}_{i,j} \tag{2.19}$$

for all $j \in \{1, \ldots, L_i\}$ and $i \in \{1, \ldots, N\}$, where $w_{i,j}^{\mathrm{low}}$ and $w_{i,j}^{\mathrm{upp}}$ denote the lower and upper bounds, respectively. The constraints in (2.19) can also be expressed in the vector form as

$$\boldsymbol{w}^{\mathrm{low}} \preceq \boldsymbol{w} \preceq \boldsymbol{w}^{\mathrm{upp}} \tag{2.20}$$

by forming $\boldsymbol{w}^{\mathrm{low}}$ and $\boldsymbol{w}^{\mathrm{upp}}$ in the same manner as $\boldsymbol{w}$, which is defined as $\boldsymbol{w} \triangleq \left[\boldsymbol{w}_1^T \ldots \boldsymbol{w}_N^T\right]^T$ with $\boldsymbol{w}_i \triangleq [w_{i,1} \cdots w_{i,L_i}]^T$. In addition to the individual power constraints in (2.20), there also exist total power constraints related to power consumption and human eye safety considerations [59], which can be stated as

$$\sum_{j=1}^{L_i} w_{i,j} \leq w_i^{\mathrm{tot}} \tag{2.21}$$

for $i = 1, \ldots, N$. The total power constraints in (2.21) can be written in the vector form as

$$\mathbf{B}\boldsymbol{w} \preceq \boldsymbol{w}^{\mathrm{tot}} \tag{2.22}$$

where $\boldsymbol{w}^{\mathrm{tot}} \triangleq [w_1^{\mathrm{tot}} \cdots w_N^{\mathrm{tot}}]^T$ and

$$\mathbf{B} \triangleq \mathrm{blkdiag}\big(\mathbf{1}_{L_1}^T, \ldots, \mathbf{1}_{L_N}^T\big) \tag{2.23}$$

with $\mathbf{1}_{L_i}$ denoting a column vector of L_i ones.

2.4 Illumination Constraints

As visible light systems are commonly utilized for illumination purposes as well, individual and average illumination constraints should also be considered. The horizontal illuminance at location $\boldsymbol{y}$ produced by the jth LED in the ith LED array can be calculated as follows [59]:

$$\mathcal{I}_{\mathrm{ind}}^{i,j}(\boldsymbol{y}, w_{i,j}) = \sqrt{w_{i,j}}\, \varphi_{i,j}(\boldsymbol{y}) \tag{2.24}$$

where

$$\varphi_{i,j}(\boldsymbol{y}) = \frac{(m_{i,j}+1)\kappa_{i,j}\tilde{E}_{i,j}^{\mathrm{opt}}}{2\pi} \frac{\big((\boldsymbol{y}-\boldsymbol{l}_{i,j})^T\boldsymbol{n}_{i,j}\big)^{m_{i,j}} (\boldsymbol{l}_{i,j}(3)-\boldsymbol{y}(3))}{\|\boldsymbol{y}-\boldsymbol{l}_{i,j}\|^{m_{i,j}+3}} \tag{2.25}$$

with $\kappa_{i,j}$ representing the luminous efficacy (lm/W) of the jth LED in the ith LED array, $\tilde{E}_{i,j}^{\text{opt}}$ denoting the optical power of the base signal in (2.1), that is, $\tilde{E}_{i,j}^{\text{opt}} \triangleq \int_0^{T_{\text{s},i}} \tilde{s}_{i,j}(t)dt/T_{\text{s},i}$, and $\boldsymbol{l}_{i,j}(3)$ and $\boldsymbol{x}(3)$ being the third components of $\boldsymbol{l}_{i,j}$ and $\boldsymbol{x}$, respectively. Therefore, the total illuminance at $\boldsymbol{y}$ generated by all the LEDs can be calculated as

$$\mathcal{I}_{\text{ind}}(\boldsymbol{y},\boldsymbol{w}) = \sum_{i=1}^{N}\sum_{j=1}^{L_i} \sqrt{w_{i,j}}\,\varphi_{i,j}(\boldsymbol{y}) = \sqrt{\boldsymbol{w}}^T\boldsymbol{\varphi}(\boldsymbol{y}) \tag{2.26}$$

with $\boldsymbol{\varphi}(\boldsymbol{y}) \triangleq [\varphi_{1,1}(\boldsymbol{y})\cdots\varphi_{1,L_1}(\boldsymbol{y})\cdots\varphi_{N,1}(\boldsymbol{y})\cdots\varphi_{N,L_N}(\boldsymbol{y})]^T$. If there exist M locations denoted by $\boldsymbol{y}_1,\ldots,\boldsymbol{y}_M$ where illuminance constraints are to be satisfied, the following set of constraints can be stated

$$\sqrt{\boldsymbol{w}}^T\boldsymbol{\varphi}(\boldsymbol{y}_\ell) \geq \tilde{\mathcal{I}}_\ell\,,\ \ell \in \{1,\ldots,M\} \tag{2.27}$$

with $\tilde{\mathcal{I}}_\ell$ specifying the illuminance constraint for location $\boldsymbol{y}_\ell$.

In addition to the individual illumination constraints in (2.27), there can also exist an average illumination constraint over a region in the positioning environment. The average illuminance can be specified as follows [59]:

$$\mathcal{I}_{\text{avg}}(\boldsymbol{w}) = \sum_{i=1}^{N}\sum_{j=1}^{L_i} \sqrt{w_{i,j}}\,\frac{\int_{\mathcal{R}}\varphi_{i,j}(\boldsymbol{y})d\boldsymbol{y}}{|\mathcal{R}|} \tag{2.28}$$

where $\mathcal{R}$ denotes the region over which the average illuminance constraint must be satisfied and $|\mathcal{R}|$ represents its volume. Then, the average illuminance constraint can be stated as

$$\sqrt{\boldsymbol{w}}^T\bar{\boldsymbol{\varphi}}_{\mathcal{R}} \geq \tilde{\mathcal{I}}_{\text{avg}} \tag{2.29}$$

where $\bar{\boldsymbol{\varphi}}_{\mathcal{R}} \triangleq |\mathcal{R}|^{-1}\big[\int_{\mathcal{R}}\varphi_{1,1}(\boldsymbol{y})d\boldsymbol{y}\cdots\int_{\mathcal{R}}\varphi_{1,L_1}(\boldsymbol{y})d\boldsymbol{y}\cdots\ \int_{\mathcal{R}}\varphi_{N,1}(\boldsymbol{y})d\boldsymbol{y}\cdots\int_{\mathcal{R}}\varphi_{N,L_N}(\boldsymbol{y})d\boldsymbol{y}\big]^T$ and $\tilde{\mathcal{I}}_{\text{avg}}$ specifies the average illuminance constraint.

2.5 Optimization Problem and Proposed Solution

Considering the power and illumination constraints given by (2.20), (2.22), (2.27), and (2.29), and the CRLB expression specified by (2.8) and (2.17), we propose the following problem for optimizing the transmit powers of the LEDs:

$$\underset{\boldsymbol{w}}{\text{minimize}}\ \text{trace}\left\{\left(\left(\mathbf{I}_3 \otimes \sqrt{\boldsymbol{w}}\right)^T \boldsymbol{H}\left(\mathbf{I}_3 \otimes \sqrt{\boldsymbol{w}}\right)\right)^{-1}\right\} \tag{2.30}$$

$$\text{subject to } \boldsymbol{w}^{\text{low}} \preceq \boldsymbol{w} \preceq \boldsymbol{w}^{\text{upp}} \tag{2.31}$$

$$\mathbf{B}\boldsymbol{w} \preceq \boldsymbol{w}^{\text{tot}} \tag{2.32}$$

$$\sqrt{\boldsymbol{w}}^T \boldsymbol{\varphi}(\boldsymbol{y}_\ell) \geq \tilde{\mathcal{I}}_\ell\,,\ \ \ell \in \{1, \ldots, M\} \tag{2.33}$$

$$\sqrt{\boldsymbol{w}}^T \bar{\boldsymbol{\varphi}}_{\mathcal{R}} \geq \tilde{\mathcal{I}}_{\text{avg}} \tag{2.34}$$

The power constraints in (2.31) and (2.32) are linear, and the illumination constraints in (2.33) and (2.34) are convex (as the left hand sides are concave functions). Therefore, the constraints specify a convex region. However, the objective function is not convex in general. Therefore, convex optimization techniques cannot directly be applied to this optimization problem to obtain its solution.

At this point, two main approaches can be considered to obtain a solution of (2.30)–(2.34). The first approach is to apply a global optimization algorithm such as particle swarm optimization (PSO) [77] to obtain a solution. However, the globally optimal solution is not guaranteed via this approach and it can have high complexity when the total number of LEDs is high. Therefore, an alternative approach is proposed as follows:

- **Step 1**: Obtain the optimal transmit power parameters that maximize the total received power at the VLC receiver under the constraints in (2.31)–(2.34) based on a *convex* optimization problem.
- **Step 2**: Use the solution of the power total maximization problem as the initial point for (2.30)–(2.34) and implement a *constrained gradient descent* algorithm to obtain the solution.

The main idea behind the proposed algorithm is that maximizing the total received power at the VLC receiver can in general improve the localization accuracy [66, Sec. III]. Therefore, it can be considered to obtain a solution that achieves a close CRLB to that achieved by the solution of the original problem in

(2.30)–(2.34). Hence, using the solution of the total received power maximization problem as an initial point, it can be possible to reach/approximate the solution of (2.30)–(2.34) via a gradient descent algorithm (although the globally optimal solution may not be guaranteed in all cases).

In Step 1 of the proposed approach, the aim is to maximize the total received power, which is given by

$$\sum_{i=1}^{N}\sum_{j=1}^{L_i} h_{i,j}\sqrt{w_{i,j}} \triangleq \sqrt{\boldsymbol{w}}^T\boldsymbol{h} \tag{2.35}$$

where $\boldsymbol{h} \triangleq \left[\boldsymbol{h}_1^T \cdots \boldsymbol{h}_N^T\right]^T$. Therefore, the following optimization problem is to be solved in Step 1:

$$\begin{aligned} &\underset{\boldsymbol{w}}{\text{maximize}}\ \sqrt{\boldsymbol{w}}^T\boldsymbol{h} \\ &\text{subject to } (2.31) - (2.34) \end{aligned} \tag{2.36}$$

It is noted that the objective function in (2.36) is a concave function of $\boldsymbol{w}$. Therefore, its maximization over the convex set of constraints in (2.31)-(2.34) leads to a convex optimization problem. Hence, this problem can be solved rapidly via convex optimization algorithms (e.g., interior point methods) to obtain its globally optimal solution [78].

Let $\boldsymbol{w}^*_{\text{init}}$ denote the solution of (2.36). Then, in Step 2 of the proposed approach, the problem in (2.30)–(2.34) is initialized with $\boldsymbol{w}^*_{\text{init}}$ and a constrained gradient descent algorithm is run for obtaining the solution. Before specifying the details of the proposed algorithm, the gradient of the objective function in (2.30) is presented in the following lemma:

Lemma: Let $C(\boldsymbol{x},\boldsymbol{w})$ denote the objective function in (2.30), i.e., the CRLB expression. Then, the partial derivative of $C(\boldsymbol{x},\boldsymbol{w})$ with respect the ℓth element of $\boldsymbol{w}$ is given by

$$\frac{\partial C(\boldsymbol{x},\boldsymbol{w})}{\partial w_\ell} = \text{trace}\left\{-\mathbf{J}^{-1}(\boldsymbol{x})\frac{\partial \mathbf{J}(\boldsymbol{x})}{\partial w_\ell}\mathbf{J}^{-1}(\boldsymbol{x})\right\} \tag{2.37}$$

where $\mathbf{J}(\boldsymbol{x})$ is as defined in (2.17) and $\frac{\partial \mathbf{J}(\boldsymbol{x})}{\partial w_\ell}$ is calculated as

$$\begin{aligned}\left[\frac{\partial \mathbf{J}(\boldsymbol{x})}{\partial w_\ell}\right]_{k_1,k_2} &= \frac{1}{2\sigma_m^2\sqrt{w_{m,\ell-\sum_{i=1}^{m-1}L_i}}}\sum_{j=1}^{L_m}\sqrt{w_{m,j}} \\ &\times\left(\frac{\partial h_{m,\ell-\sum_{i=1}^{m-1}L_i}}{\partial x_{k_1}}\frac{\partial h_{m,j}}{\partial x_{k_2}}+\frac{\partial h_{m,\ell-\sum_{i=1}^{m-1}L_i}}{\partial x_{k_2}}\frac{\partial h_{m,j}}{\partial x_{k_1}}\right)\end{aligned}\tag{2.38}$$

if $\ell \in \left\{\sum_{i=1}^{m-1}L_i+1,\ldots,\sum_{i=1}^{m}L_i\right\}$ for $m\in\{1,\ldots,N\}$, with $k_1,k_2\in\{1,2,3\}$.

Proof: Since the CRLB is given by $C(\boldsymbol{x},\boldsymbol{w}) = \mathrm{trace}\left\{\mathbf{J}^{-1}(\boldsymbol{x})\right\}$, its partial derivative with respect to w_ℓ can be expressed as in (2.37) [79]. Then, the partial derivative of $\mathbf{J}(\boldsymbol{x})$ with respect to w_ℓ can be obtained based on (2.11) after some manipulation as follows:

$$\begin{aligned}\left[\frac{\partial \mathbf{J}(\boldsymbol{x})}{\partial w_\ell}\right]_{k_1,k_2} &= \frac{1}{2\sigma_m^2\sqrt{w_{m,\ell-\sum_{i=1}^{m-1}L_i}}} \\ &\times\left(\frac{\partial h_{m,\ell-\sum_{i=1}^{m-1}L_i}}{\partial x_{k_1}}\sum_{j=1}^{L_m}\sqrt{w_{m,j}}\frac{\partial h_{m,j}}{\partial x_{k_2}}\right. \\ &\left.+\frac{\partial h_{m,\ell-\sum_{i=1}^{m-1}L_i}}{\partial x_{k_2}}\sum_{j=1}^{L_m}\sqrt{w_{m,j}}\frac{\partial h_{m,j}}{\partial x_{k_1}}\right)\end{aligned}\tag{2.39}$$

if $\ell \in \left\{\sum_{i=1}^{m-1}L_i+1,\ldots,\sum_{i=1}^{m}L_i\right\}$ for $m\in\{1,\ldots,N\}$ where $k_1,k_2\in\{1,2,3\}$. Then, reorganizing the terms in the parentheses in (2.39) yields the expression in (2.38). □

Based on (2.37) and (2.38) in the Lemma, the gradient of the objective function in (2.30) can be obtained as

$$\nabla_{\boldsymbol{w}}C(\boldsymbol{x},\boldsymbol{w}) = \left[\frac{\partial C(\boldsymbol{x},\boldsymbol{w})}{\partial w_1}\cdots\frac{\partial C(\boldsymbol{x},\boldsymbol{w})}{\partial w_{\sum_{i=1}^{N}L_i}}\right]^T . \tag{2.40}$$

By using the gradient of the objective function, Algorithm 1 presented below is implemented to obtain a solution of (2.30)–(2.34).

The projection operation in line 9 of Algorithm 1 is performed to keep the solution in the feasible region, which is a common approach for constrained gradient descent algorithms called *projected gradient descent* [78]. It is noted that

Algorithm 1

Let ζ and T denote, respectively, the step size and the number of steps for gradient descent.
Let $\mathcal{S}$ denote the set of $\boldsymbol{w}$ that satisfy (2.31)–(2.34).
Solve (2.36) via an interior point algorithm [78] and obtain its solution denoted by $\boldsymbol{w}^*_{\text{init}}$.
$\boldsymbol{w}^{(0)} \leftarrow \boldsymbol{w}^*_{\text{init}}$
$\boldsymbol{w}_{\text{opt}} \leftarrow \boldsymbol{w}^{(0)}$
for $t = 1$ to T **do**
    $\boldsymbol{w}^{(t)} \leftarrow \boldsymbol{w}^{(t-1)} - \zeta \, \nabla_{\boldsymbol{w}} C(\boldsymbol{x}, \boldsymbol{w}^{(t-1)})$
    if $\boldsymbol{w}^{(t)} \notin \mathcal{S}$ **then**
        $\boldsymbol{w}^{(t)} \leftarrow \arg\min_{\boldsymbol{w} \in \mathcal{S}} \|\boldsymbol{w}^{(t)} - \boldsymbol{w}\|$
    end if
    if $C(\boldsymbol{x}, \boldsymbol{w}^{(t)}) < C(\boldsymbol{x}, \boldsymbol{w}_{\text{opt}})$ **then**
        $\boldsymbol{w}_{\text{opt}} \leftarrow \boldsymbol{w}^{(t)}$
    end if
end for
Return $\boldsymbol{w}_{\text{opt}}$.

this projection operation corresponds to a convex optimization problem since $\mathcal{S}$ is a convex set and the objective function is convex.

In contrast to brute-force heuristics such as particle swarm optimization, the proposed method offers a structured and efficient framework. The employment of brute-force methods carries a risk of the algorithm being trapped in local optimum points, thereby providing no guarantee of optimality. Moreover, as the number of LEDs and LED arrays increases in the VLP system, these methods become computationally intensive, and their performance degrades in the high-dimensional search space [80]. The proposed approach exploits the problem structure directly, enabling faster convergence and more effective scaling to high-dimensional LED array configurations, which makes it more robust and practical than brute force methods for VLP systems.

The complexity of Algorithm 1 is mainly determined by the complexity of solving the convex optimization problems for projection (which occurs at most T times, with T denoting the number of steps in the gradient descent algorithm), and the calculations of the gradient in line 7 and the CRLB in line 11 of Algorithm 1. In general, the CRLB and gradient calculations have lower computational complexity than the projection operation in line 9 since their complexity mainly depends on the complexity of 3×3 matrix inversion (please see (2.30) and (2.37)) whereas the projection operation involves convex optimization over a $\sum_{i=1}^{N} L_i$ dimensional space with $\sum_{i=1}^{N} L_i$ being a large number in most practical cases (e.g., 16 in the simulations in Section 3.1). Considering the interior point method for solving the convex optimization problem, the projection operation has a worst-case complexity of $\mathcal{O}((\sum_{i=1}^{N} L_i)^3)$.

2.6 Iterative Power Allocation and Localization for Practical Implementation

The optimization problem formulated and solved in Section 2.5 requires the knowledge of the location $\boldsymbol{x}$ of the VLC receiver, which is not available in practice. For *tracking* applications, the position estimate of the VLC receiver in the previous time step can be employed to implement the proposed algorithm (Algorithm 1). Then, the obtained power parameter vector $\boldsymbol{w}$ can be used to transmit signals from the LEDs (please see (2.1)) and the resulting received powers, denoted by $P_{\mathrm{RX},1}, \ldots, P_{\mathrm{RX},N}$, are observed as in (2.4). Based on these received powers, the ML estimator, which can be obtained from (2.7), is implemented as follows:

$$\begin{aligned}\hat{\boldsymbol{x}} &= \arg\min_{\boldsymbol{x}} \sum_{i=1}^{N} \frac{1}{\sigma_i^2} \left(P_{\mathrm{RX},i} - \sum_{j=1}^{L_i} h_{i,j} \sqrt{w_{i,j}} \right)^2 \\ &\triangleq \arg\min_{\boldsymbol{x}} \tilde{G}(\boldsymbol{P}_{\mathrm{RX}}, \boldsymbol{w}) \end{aligned} \tag{2.41}$$

where $h_{i,j}$ is a function of $\boldsymbol{x}$ as specified in (2.6), $w_{i,j}$'s correspond to the elements of $\boldsymbol{w}$; that is, $\boldsymbol{w} = \left[w_{1,1} \cdots w_{1,L_1} \cdots w_{N,1} \cdots w_{N,L_N}\right]^T$, and $\boldsymbol{P}_{\mathrm{RX}} = [P_{\mathrm{RX},1} \ldots P_{\mathrm{RX},N}]^T$, as defined before.

In the absence of tracking (i.e., without any prior knowledge about the position of the VLC receiver), localization and power allocation can be performed in an iterative manner by implementing the following N_{S}-step algorithm, called Algorithm 2.

For the random initialization of the power parameter vector in Algorithm 2, one reasonable choice can be uniform (equal) power allocation, i.e., $w_{i,j} = w_i^{\mathrm{tot}}/L_i$ for $j = 1, \ldots, L_i$ and $i = 1, \ldots, N$ if it is feasible (that is, if it satisfies (2.31)–(2.34)). Also, as the noise variances decay to zero, the performance of the position estimator in Algorithm 2 is expected to converge, in a few iterations, to that of the ML estimator which is based on the power parameter vector obtained by assuming the knowledge of the position of the VLC receiver (i.e., obtained via Algorithm 1). This expectation stems from the asymptotic optimality properties

Algorithm 2

for $k = 1$ to N_{S} **do**
    if $k = 1$ **then**
        Set $\boldsymbol{w}$ randomly to a point $\boldsymbol{w}^{(1)}$ in feasible region specified by (2.31)–(2.34).
    else
        Use $\hat{\boldsymbol{x}}^{(k-1)}$ as the VLC receiver position and implement Algorithm 1 to obtain the power parameters, which are denoted by $\boldsymbol{w}^{(k)}$.
    end if
    Transmit signals from the LED arrays according to the power parameters in $\boldsymbol{w}^{(k)}$ (see (2.1)). Let the corresponding received powers in (2.4) be denoted by $\boldsymbol{P}_{\mathrm{RX}}^{(k)} = [P_{\mathrm{RX},1}^{(k)}, \ldots, P_{\mathrm{RX},N}^{(k)}]$.
    Implement the ML estimator for the position of the VLC receiver based on $\boldsymbol{P}_{\mathrm{RX}}^{(k)}$ and $\boldsymbol{w}^{(k)}$ as follows:

$$\hat{\boldsymbol{x}}^{(k)} = \arg\min_{\boldsymbol{x}} \tilde{G}\big(\boldsymbol{P}_{\mathrm{RX}}^{(k)}, \boldsymbol{w}^{(k)}\big) \tag{2.42}$$

    with $\tilde{G}(\cdot)$ being defined as in (2.41).
end for
Return $\boldsymbol{w}_{\mathrm{opt}}$ and $\hat{\boldsymbol{x}}^{(N_{\mathrm{S}})}$.

of the ML estimator [66, 76].

Since Algorithm 2 employs Algorithm 1 in each iteration, its complexity burden on the VLP system for setting the parameters of the LED arrays is $(N_{\mathrm{S}}-1)$ times that of Algorithm 1 (-1 is due to the use of the random (or, uniform) power allocation approach in the initial step). On the other hand, the ML estimator is implemented at the VLC receiver as in (2.42), solving which requires a $3-$dimensional search over the indoor environment. (Since $\tilde{G}$ is not a convex function of $\boldsymbol{x}$, exhaustive search with a certain resolution can be performed.). It should also be noted that the VLC receiver informs the VLP network about its ML position estimate so that the power allocation can be optimized for the next iteration.

Chapter 3

Performance Analysis of the Proposed Approaches

In this chapter, we present simulation results to illustrate the improvements achieved through the proposed power allocation approach and the iterative power allocation and localization approach. Firstly, we describe the indoor environment in which the simulations are executed. Then, we present the results of the simulations and provide an analysis of the performances of the proposed methods.

3.1 Setup Description

The indoor localization environment considered in the simulations is a room with dimensions $20 \times 20 \times 5\,\mathrm{m}^3$, where the lower left corner of the room is considered as the origin, $[0\ 0\ 0]^T$, as shown in Fig. 3.1. There exist $N = 4$ LED arrays on the ceiling of the room, which are centered at $[5\ 5\ 5]^T$ m, $[15\ 5\ 5]^T$ m, $[5\ 15\ 5]^T$ m, and $[15\ 15\ 5]^T$ m for LED arrays 1, 2, 3, and 4, respectively.

Each LED array consists of four LEDs, i.e., $L_i = 4$ for $i = 1, 2, 3, 4$. The four LEDs in each array are placed with a distance of ± 5 cm with respect to the

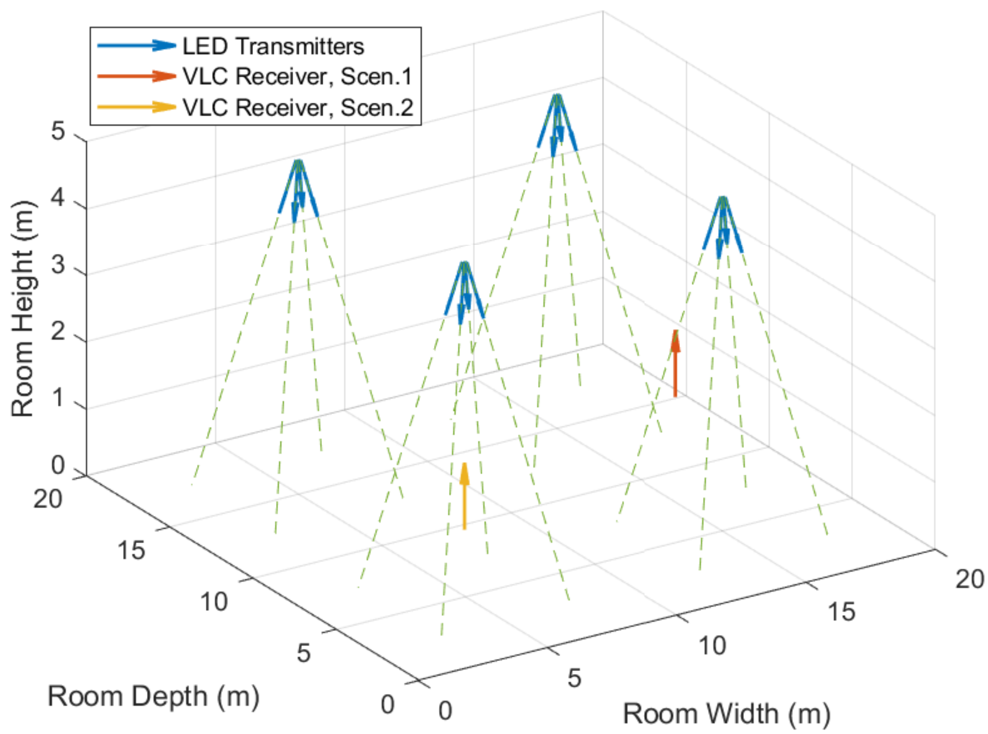

Figure 3.1: VLP system considered in the simulations, where there exist 4 LED arrays each consisting of 4 LEDs. The VLC receiver is placed at two different locations in Scenario 1 and Scenario 2 as shown in the figure. The dashed lines are used to illustrate the orientation vectors of the LEDs more clearly.

center of the LED array in the x and y directions. In particular, the locations of the LEDs in LED array 1 are $\boldsymbol{l}_{1,1} = [5.05\ 5.05\ 5]^T$, $\boldsymbol{l}_{1,2} = [5.05\ 4.95\ 5]^T$, $\boldsymbol{l}_{1,3} = [4.95\ 5.05\ 5]^T$, and $\boldsymbol{l}_{1,4} = [4.95\ 4.95\ 5]^T$ m. Similarly, the locations of the LEDs in LED array 2 are $\boldsymbol{l}_{2,1} = [15.05\ 5.05\ 5]^T$, $\boldsymbol{l}_{2,2} = [15.05\ 4.95\ 5]^T$, $\boldsymbol{l}_{2,3} = [14.95\ 5.05\ 5]^T$, and $\boldsymbol{l}_{2,4} = [14.95\ 4.95\ 5]^T$ m, those in LED array 3 are $\boldsymbol{l}_{3,1} = [5.05\ 15.05\ 5]^T$, $\boldsymbol{l}_{3,2} = [5.05\ 14.95\ 5]^T$, $\boldsymbol{l}_{3,3} = [4.95\ 15.05\ 5]^T$, and $\boldsymbol{l}_{3,4} = [4.95\ 14.95\ 5]^T$ m, and those in LED array 4 are $\boldsymbol{l}_{4,1} = [15.05\ 15.05\ 5]^T$, $\boldsymbol{l}_{4,2} = [15.05\ 14.95\ 5]^T$, $\boldsymbol{l}_{4,3} = [14.95\ 15.05\ 5]^T$, and $\boldsymbol{l}_{4,4} = [14.95\ 14.95\ 5]^T$ m. It is noted that the LED arrays are placed at the centers of the four $10\,\text{m} \times 10\,\text{m}$ squares that divide the ceiling of the room into four equal areas. The orientation vectors of the LEDs in the LED arrays are arranged such that each LED is pointed towards the closest of the 16 points which correspond to the centers the $5\,\text{m}\times 5\,\text{m}$ squares on the floor shown in Fig. 3.1. For example, the LED at location $\boldsymbol{l}_{1,1} = [5.05\ 5.05\ 5]^T$m is oriented towards $[7,5\ 7.5\ 0]^T$m. Due to the symmetry, the LEDs in each array have the same set of four orientation vectors, which can be calculated as $\boldsymbol{n}_{i,1} = [0.4028\, 0.4028\ -0.8219]^T$, $\boldsymbol{n}_{i,2} = [0.4028\ -0.4028\ -0.8219]^T$, $\boldsymbol{n}_{i,3} = [-0.4028\ 0.4028\ -0.8219]^T$, and $\boldsymbol{n}_{i,4} = [-0.4028\ -0.4028\ -0.8219]^T$ for $i = 1, 2, 3, 4$. The setup of the LED arrays is illustrated in Fig. 3.1, where the dashed lines are used to demonstrate the orientations of the LEDs.

To investigate the performance of the proposed approaches in different conditions, we consider two scenarios for the location of the VLC receiver. In *Scenario 1*, the VLC receiver is placed at $\boldsymbol{x} = [14\ 6.3\ 1.9]^T$ m while it is at $\boldsymbol{x} = [5\ 5\ 1]^T$ m in *Scenario 2*. In both scenarios, the orientation vector of the VLC receiver is given by $\bar{\boldsymbol{n}} = [0\ 0\ 1]$, i.e., it has a perpendicular orientation. The location and the orientation of the VLC receiver are shown in Fig. 3.1 for each scenario. Since the LEDs in the LED arrays have various locations and orientations, some of them may not be in the field of view (FOV) of the VLC receiver in a given scenario. Specifically, in *Scenario 1*, the jth LED of the ith LED array is not in the FOV of the VLC receiver if $(i, j) \in \{(1, 3), (1, 4), (3, 3), (4, 1), (4, 3)\}$ while all the other LEDs are in the FOV. Similarly, the LEDs that are not in the FOV of the VLC receiver in *Scenario 2* are specified by indices $(i, j) \in \{(2, 1), (2, 2), (3, 1), (3, 3), (4, 1)\}$, where i and j

Table 3.1: Simulation parameters.

Responsivity of photo-detector, R_p	0.4 mA/mW
Area of photo-detector, A	1 cm^2
Noise spectral density level, σ^2	10^{-15} W/Hz
LED Lambertian order, $m_{i,j},\ \forall i,j$	1
LED luminous efficacy, $\kappa_{i,j},\ \forall i,j$	284 lm/W
Min. LED optical power parameter, $w_{i,j}^{\text{low}},\ \forall i,j$	5 W
Max. LED optical power parameter, $w_{i,j}^{\text{upp}},\ \forall i,j$	20 W
Individual illuminance limit, $\tilde{\mathcal{I}}_\ell,\ \ell = 1,2,3,4$	30 lx
Average illuminance limit, $\tilde{\mathcal{I}}_{\text{avg}}$	30 lx

denote the indices of the LED array and the LED, respectively. Regarding the individual illumination constraints in (2.33), $M = 4$ locations are specified as $\boldsymbol{y}_1 = [5\ 5\ 1]^T$ m, $\boldsymbol{y}_2 = [15\ 5\ 1]^T$ m, $\boldsymbol{y}_3 = [5\ 15\ 1]^T$ m, and $\boldsymbol{y}_4 = [15\ 15\ 1]^T$ m. Hence, certain illumination levels should be guaranteed at these four locations. On the other hand, the average illumination of the room is computed as specified in (2.28) and the computation is performed over the horizontal plane of the room the height of which is set at 1 m. Moreover, in accordance with [59], [81] and [82], the VLP system parameters employed in the simulations are given in Table 3.1 [59, 81, 82].

In the simulations, the total power constraints for the LED arrays are taken to be equal, i.e., $w_i^{\text{tot}} = w^{\text{tot}}$, for $i = 1, 2, 3, 4$. To provide a comparative performance evaluation of Algorithm 1, the transmit power parameters are calculated based on the following three approaches: (i) Uniform (equal) transmit power parameters (i.e., $w_{i,j} = w^{\text{tot}}/L_i$ for $i, j = 1, 2, 3, 4$), (ii) Power maximization approach in (2.34), which is solved via CVX in Matlab, and (iii) Algorithm 1 specified in Section 2.5. Then, the CRLBs achieved by using these transmit power parameters are obtained. In addition, the root-mean squared errors (RMSEs) of the ML estimators in (2.41) are calculated when the transmit power parameters obtained from these three approaches are used. Fig. 3.2 and Fig. 3.3 illustrate the CRLBs and the RMSEs of the ML estimators for these three approaches versus w^{tot} considering the two scenarios for the location of the VLC receiver.

3.2 Performance of Algorithm 1

Fig. 3.2 demonstrates that when the VLC receiver is placed as in Scenario 1, the proposed approach can yield substantial enhancements in comparison to the

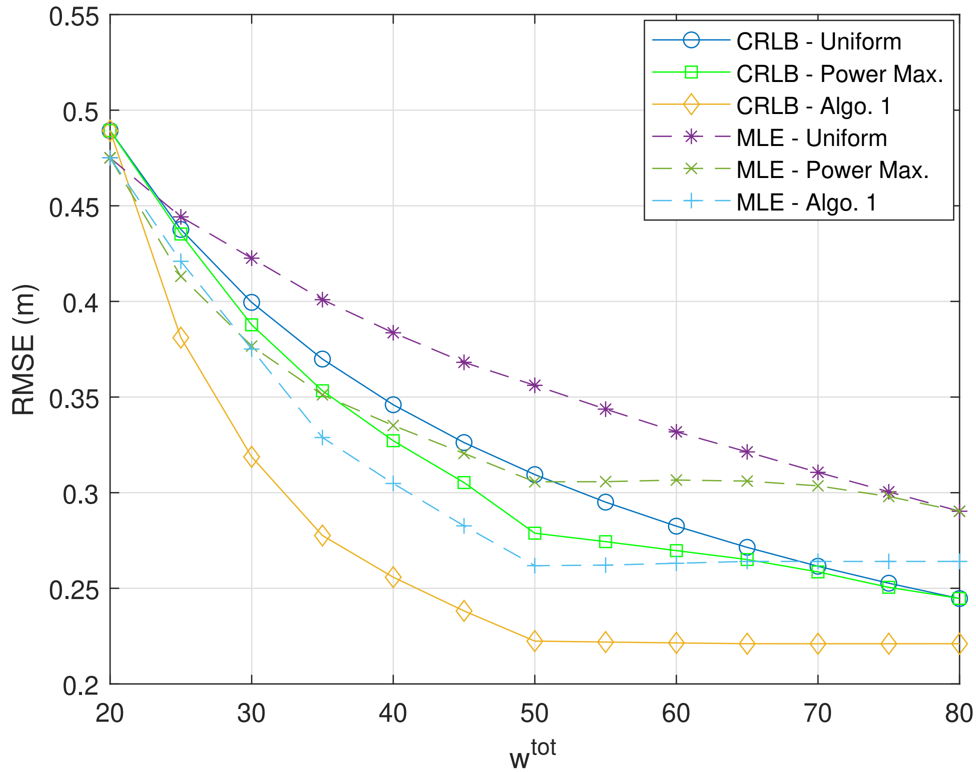

Figure 3.2: RMSEs of the ML estimators and the CRLBs corresponding to uniform, power maximization and proposed (Algorithm 1) power allocation strategies with respect to w^{tot} for Scenario 1.

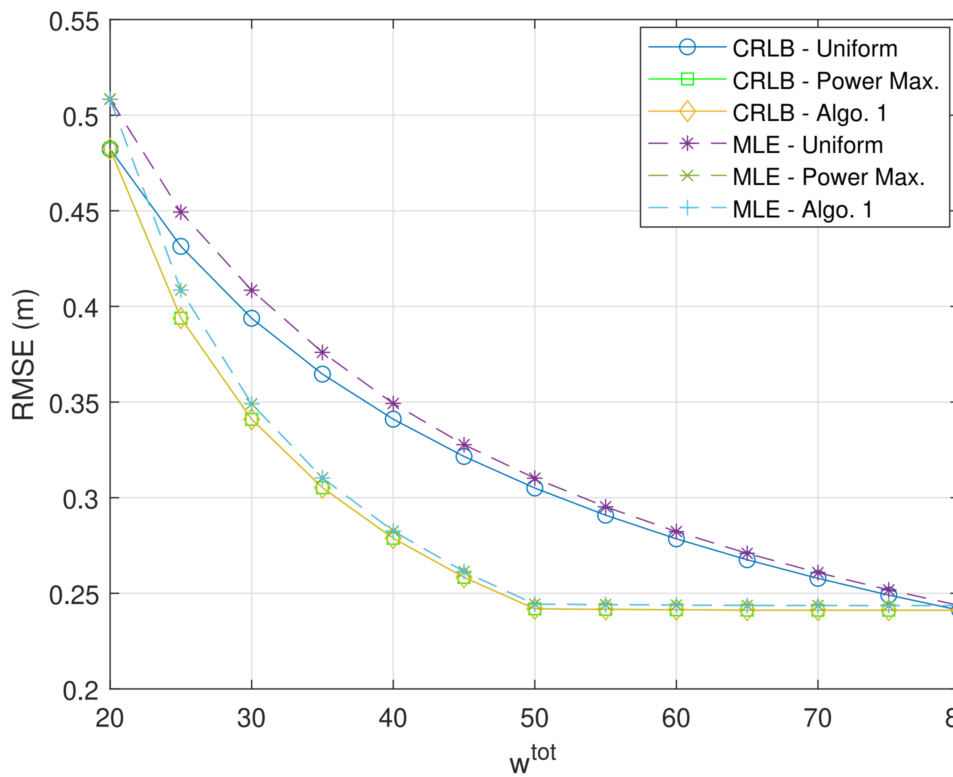

Figure 3.3: RMSEs of the ML estimators and the CRLBs corresponding to uniform, power maximization and proposed (Algorithm 1) power allocation strategies with respect to w^{tot} for Scenario 2.

power optimization approach and the conventional uniform power allocation approach in terms of both the CRLB and ML estimation performance.[1] These enhancements are more pronounced at higher values of w^{tot} since all the approaches yield the same result of assigning 5 to all the transmit power parameters when $w^{\text{tot}} = 20$ (since $w_{i,j}^{\text{low}} = 5$ and $w_{i,j}^{\text{upp}} = 20$ for all i, j). From the results in Fig. 3.2, it is inferred that maximizing the received power at the VLC receiver location does not always lead to the optimal localization performance. For further elaboration, Table 3.2 presents the transmit power parameters obtained from the power maximization approach and Algorithm 1 for Scenario 1 when w^{tot} is set to 40 and 60. Upon the examination of the values in the table, it is observed that although both of the approaches yield similar values for LED array 1, LED array 3, and LED array 4, the transmit power parameters for LED array 2 are significantly different. It is noted that LED array 2 is the closest LED array to the VLC receiver in Scenario 1. The proposed approach (Algorithm 1) prioritizes maximizing the transmit power parameter of the second LED of that array over others, while ensuring that the transmit power parameters of the first and third LEDs of the array are maintained at their minimum. It is important to note that when $w^{\text{tot}} = 60$, the transmit power parameter set for LED array 2 is $(5, 20, 5, 20)$ according to Algorithm 1, resulting in a total power of 50, which is lower than the specified total power constraint of 60. The underlying cause of this phenomenon can be attributed to the fact that the efficacy of the localization process is contingent upon the power sensitivity of the power measurements with respect to the the location of the VLC receiver; hence, it depends on the partial derivatives in (2.12). Since these partial derivatives can have opposite signs for different LEDs in a given array, increasing the power of an LED can sometimes have a destructive effect on the localization performance [66]. Due to this behavior, the proposed approach (Algorithm 1) converges to its optimal value at around $w^{\text{tot}} = 50$. Increasing the total power constraint above this level does not significantly improve the CRLB as seen in Fig. 3.2. In Table 3.2, the transmit power parameters of

[1] Since the possible locations for the VLC receiver within the room are constrained to a volume of $20 \times 20 \times 5\,\text{m}^3$, the ML estimator conducts a search within this designated space. On the other hand, the CRLB derivations do not presume any a-priori knowledge about the location of the VLC receiver. Hence, the RMSEs of the ML estimator may be lower than the CRLBs in noisy cases as in Fig. 3.2.

Table 3.2: Transmit power parameters obtained from the power maximization approach and Algorithm 1 for Scenario 1. The transmit parameters of the LEDs that are not in the FOV of the VLC receiver in Scenario 1 are indicated with blue color.

	$(w_{1,1}, w_{1,2}, w_{1,3}, w_{1,4})$	$(w_{2,1}, w_{2,2}, w_{2,3}, w_{2,4})$	$(w_{3,1}, w_{3,2}, w_{3,3}, w_{3,4})$	$(w_{4,1}, w_{4,2}, w_{4,3}, w_{4,4})$
Power max., $w^{\text{tot}} = 40$	$(17.6, 12.4, 5, 5)$	$(9.64, 5, 17.57, 7.79)$	$(8.14, 20, 5, 6.86)$	$(5, 12.95, 5, 17.05)$
Algorithm 1, $w^{\text{tot}} = 40$	$(17.6, 12.4, 5, 5)$	$(5, 20, 5, 10)$	$(8.14, 20, 5, 6.86)$	$(5, 13.51, 5, 16.49)$
Power max., $w^{\text{tot}} = 60$	$(20, 20, 9.16, 9.14)$	$(18.68, 6.22, 20, 15.1)$	$(18.6, 20, 5, 16.4)$	$(9.14, 20, 9.16, 20)$
Algorithm 1, $w^{\text{tot}} = 60$	$(20, 20, 9.16, 9.14)$	$(5, 20, 5, 20)$	$(18.6, 20, 5, 16.4)$	$(9.14, 20, 9.16, 20)$

the LEDs that are not in the FOV of the VLC receiver in Scenario 1 are marked with blue color. In most cases, the minimum transmit power parameter of 5 is assigned to those LEDs. However, when $w^{\text{tot}} = 60$ and the transmit power parameters of the other LEDs are at the maximum level of 20, the LEDs outside the FOV can be assigned any transmit power parameter value within the feasible region (for example, $[5, 10]$ for $w_{1,3}, w_{1,4}, w_{4,1}, w_{4,3}$) as these LEDs do not affect the CRLB value. Hence, the transmit power parameters presented in the table for those LEDs do not correspond to unique solutions.

It is also possible that the performance of the proposed approach (Algorithm 1) can be equivalent to the power maximization approach in certain instances, as illustrated in Fig. 3.3, where the location of the VLC receiver is set as in Scenario 2. In this scenario, maximizing the received power at the VLC receiver is equivalent to CRLB minimization and yields the optimal solution. Table 3.3 provides the transmit power parameters obtained from the power maximization approach and Algorithm 1 for Scenario 2 with w^{tot} being set to 40 and 60. As demonstrated in the table, it is evident that the two approaches result in the same transmit power parameters. However, they still demonstrate superiority over the uniform power allocation as noted from Fig. 3.3. Also, similar to Table 3.2, the transmit power parameters of the LEDs that are not in the FOV of the VLC receiver in Scenario 2 are marked with blue color in Table 3.3, and $w_{2,1}, w_{2,2}, w_{3,1}, w_{3,3}$ are not unique for $w^{\text{tot}} = 60$.

3.3 Performance of Algorithm 2

Fig. 3.4 and Fig. 3.5 illustrate the RMSE values of the ML estimators implemented in the iterations of Algorithm 2 along with the RMSEs of the ML estimators of Algorithm 1 (the case of known VLC receiver location) with respect to w^{tot} for the two scenarios. It is observed from these figures that, despite the initial position of the receiver being unknown in Algorithm 2, the results produced by it are comparable to those of Algorithm 1 after a few iterations. Fig. 3.4, which corresponds to Scenario 1, demonstrates that the performance of Algorithm 2 gets

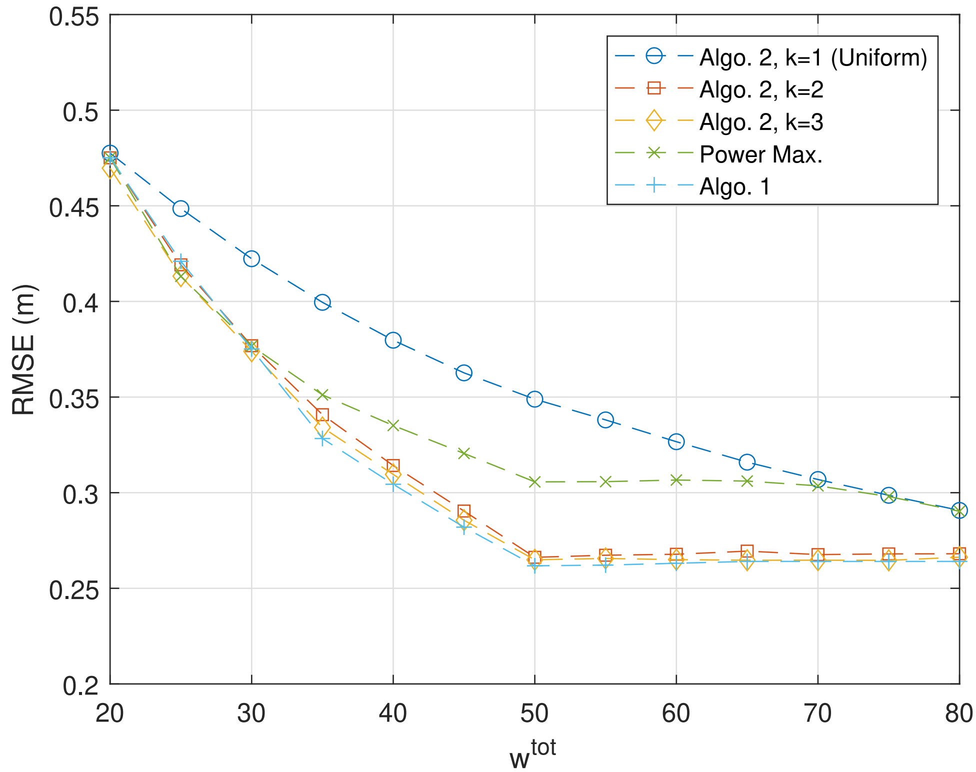

Figure 3.4: RMSEs of the ML estimators corresponding to uniform, power maximization and the two proposed power allocation strategies (Algorithm 1 and Algorithm 2) with respect to w^{tot} for Scenario 1.

Table 3.3: Transmit power parameters obtained from the power maximization approach and Algorithm 1 for Scenario 2. The transmit parameters of the LEDs that are not in the FOV of the VLC receiver in Scenario 2 are indicated with blue color.

	$(w_{1,1}, w_{1,2}, w_{1,3}, w_{1,4})$	$(w_{2,1}, w_{2,2}, w_{2,3}, w_{2,4})$	$(w_{3,1}, w_{3,2}, w_{3,3}, w_{3,4})$	$(w_{4,1}, w_{4,2}, w_{4,3}, w_{4,4})$
Power max., $w^{\text{tot}} = 40$	$(10, 10, 10, 10)$	$(5, 5, 15, 15)$	$(5, 15, 5, 15)$	$(5, 7.5, 7.5, 20)$
Algorithm 1, $w^{\text{tot}} = 40$	$(10, 10, 10, 10)$	$(5, 5, 15, 15)$	$(5, 15, 5, 15)$	$(5, 7.5, 7.5, 20)$
Power max., $w^{\text{tot}} = 60$	$(15, 15, 15, 15)$	$(9.15, 9.12, 20, 20)$	$(9.15, 20, 9.12, 20)$	$(5, 17.5, 17.5, 20)$
Algorithm 1, $w^{\text{tot}} = 60$	$(15, 15, 15, 15)$	$(9.15, 9.12, 20, 20)$	$(9.15, 20, 9.12, 20)$	$(5, 17.5, 17.5, 20)$

very close to that of Algorithm 1 in the third iteration. Notably, even in the second iteration, a substantial enhancement in the performance of the proposed method (Algorithm 2) is evident when compared to both the uniform power allocation and power maximization approaches. On the other hand, as illustrated in Fig. 3.5, when the location of the VLC receiver is as in Scenario 2, the performance of Algorithm 2 converges to that of Algorithm 1 in the second iteration. The third iteration is omitted from the figure since convergence is already achieved in the second iteration.

In summary, Algorithm 2 is shown to provide a viable solution for practical cases in which the location of the VLC receiver is unknown. These results demonstrate the practicability and efficacy of the proposed approach, suggesting its potential for successful implementation in practical settings.

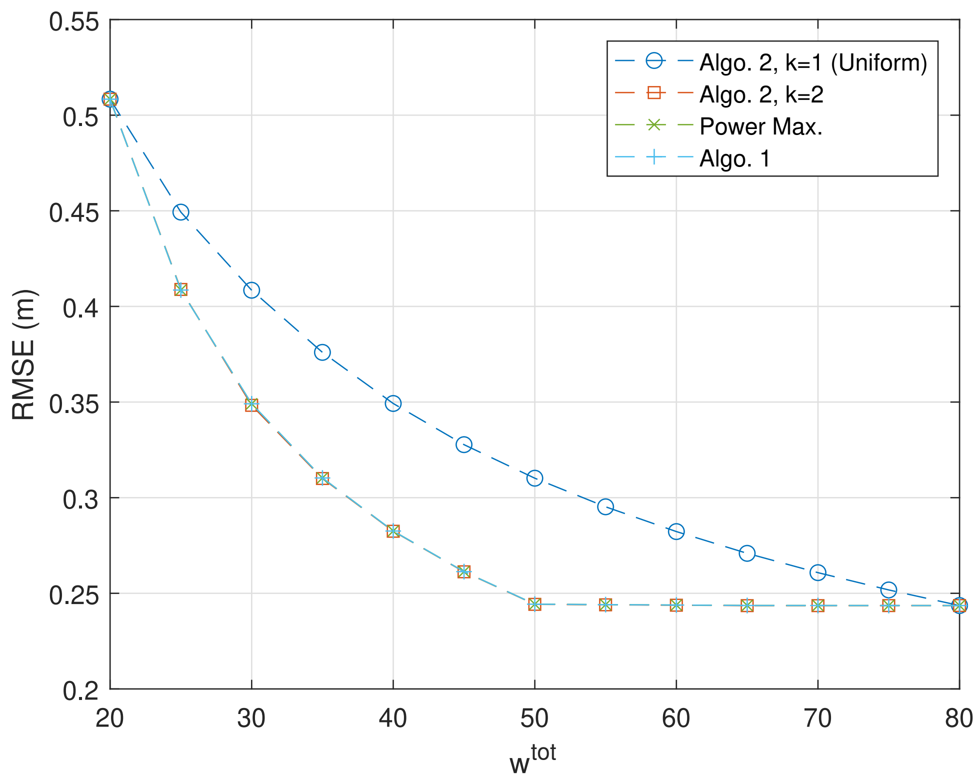

Figure 3.5: RMSEs of the ML estimators corresponding to uniform, power maximization and the two proposed power allocation strategies (Algorithm 1 and Algorithm 2) with respect to w^{tot} for Scenario 2.

Chapter 4

Conclusion and Future Work

In this thesis, we presented a power allocation framework for asynchronous VLP systems using LED arrays, with consideration of practical power and illumination constraints. The proposed approach involved the formulation and solution of a constrained optimization problem for minimizing the CRLB for the receiver location while satisfying the constraints imposed by illumination requirements and power limitations. Our two-step algorithm, which first maximizes the total received power via convex optimization and then refines the power parameters with a projected gradient descent approach, proved effective and practical, especially when integrated with an iterative localization procedure. Simulation results confirmed that the proposed power allocation strategy consistently attains superior positioning accuracy in comparison to uniform or purely power-based methods, illustrating its significance for indoor localization applications.

There are several directions in which the framework can be extended in future research. Designs that integrate positioning and data communication objectives within a single power budget are a natural extension, particularly for lighting infrastructures that require guidance and connectivity. Moreover, learning-based methods can be introduced to the framework, and a hybrid VLP approach can be developed to enhance the performance of the proposed methods and increase precision.

Bibliography

[1] H. Liu, H. Darabi, P. Banerjee, and J. Liu, "Survey of wireless indoor positioning techniques and systems," *IEEE Transactions on Systems, Man and Cybernetics, Part C (Applications and Reviews)*, vol. 37, p. 1067–1080, Nov 2007.

[2] R. Mautz, *Indoor Positioning Technologies.* PhD thesis, ETH Zürich, 2012.

[3] J. Hightower and G. Borriello, "Location systems for ubiquitous computing," *Computer*, vol. 34, pp. 57–66, 1 2001.

[4] F. Zafari, A. Gkelias, and K. K. Leung, "A survey of indoor localization Systems and technologies," *IEEE Communications Surveys & Tutorials*, vol. 21, pp. 2568–2599, 1 2019.

[5] A. Basiri, E. S. Lohan, T. Moore, A. Winstanley, P. Peltola, C. Hill, P. Amirian, and P. F. E. Silva, "Indoor location based services challenges, requirements and usability of current solutions," *Computer Science Review*, vol. 24, pp. 1–12, 4 2017.

[6] A. Tasdelen and A. Ozpinar, "OHS 4.0 approach and use case of indoor positioning systems," *2020 4th International Symposium on Multidisciplinary Studies and Innovative Technologies (ISMSIT)*, pp. 1–5, 10 2020.

[7] M. N. K. Boulos and G. Berry, "Real-time locating systems (RTLS) in healthcare: a condensed primer," *International Journal of Health Geographics*, vol. 11, p. 25, 1 2012.

[8] A. Morar, A. Moldoveanu, I. Mocanu, F. Moldoveanu, I. E. Radoi, V. Asavei, A. Gradinaru, and A. Butean, “A comprehensive survey of indoor localization methods based on computer vision,” *Sensors*, vol. 20, p. 2641, 5 2020.

[9] R. F. Brena, J. P. García-Vázquez, C. E. Galván-Tejada, D. Muñoz-Rodriguez, C. Vargas-Rosales, and J. Fangmeyer, “Evolution of Indoor Positioning Technologies: A survey,” *Journal of Sensors*, vol. 2017, pp. 1–21, 1 2017.

[10] P. Bahl and V. Padmanabhan, “Radar: An in-building RF-based user location and tracking system,” *Proceedings IEEE INFOCOM 2000. Conference on Computer Communications. Nineteenth Annual Joint Conference of the IEEE Computer and Communications Societies (Cat. No.00CH37064)*, vol. 2, p. 775–784, 2000.

[11] S. Bastiaens, J. Van-Vlaenderen Gerwen, N. Macoir, K. Deprez, C. De Cock, W. Joseph, E. De Poorter, and D. Plets, “Experimental benchmarking of next-gen indoor positioning technologies: (unmodulated) visible light positioning and ultra-wideband,” *IEEE Internet of Things Journal*, vol. 9, no. 18, pp. 17858–17870, 2022.

[12] S. He and S.-h. G. Chan, “Wi-Fi Fingerprint-Based Indoor Positioning: Recent Advances and Comparisons,” *IEEE Communications Surveys & Tutorials*, vol. 18, pp. 466–490, 8 2015.

[13] R. Faragher and R. Harle, “An analysis of the accuracy of Bluetooth low Energy for indoor positioning applications,” *Proceedings of the 27th International Technical Meeting of The Satellite Division of the Institute of Navigation (ION GNSS+ 2014)*, pp. 201–210, 9 2014.

[14] A. Alarifi, A. Al-Salman, M. Alsaleh, A. Alnafessah, S. Al-Hadhrami, M. Al-Ammar, and H. Al-Khalifa, “Ultra wideband indoor positioning Technologies: analysis and recent advances,” *Sensors*, vol. 16, p. 707, 5 2016.

[15] N. Kbayer and M. Sahmoudi, “Performances Analysis of GNSS NLOS bias correction in urban environment using a Three-Dimensional city model and

GNSS simulator," *IEEE Transactions on Aerospace and Electronic Systems*, vol. 54, pp. 1799–1814, 2 2018.

[16] J. Armstrong, Y. Sekercioglu, and A. Neild, "Visible light positioning: A roadmap for international standardization," *IEEE Communications Magazine*, vol. 51, p. 68–73, Dec 2013.

[17] S. Monica and G. Ferrari, "UWB-based localization in large indoor scenarios: optimized placement of anchor nodes," *IEEE Transactions on Aerospace and Electronic Systems*, vol. 51, pp. 987–999, 4 2015.

[18] Y. Zhuang, L. Hua, L. Qi, J. Yang, P. Cao, Y. Cao, Y. Wu, J. Thompson, and H. Haas, "A survey of positioning systems using visible LED lights," *IEEE Communications Surveys & Tutorials*, vol. 20, pp. 1963–1988, 1 2018.

[19] X. Cao, Y. Zhuang, G. Chen, X. Wang, X. Yang, and B. Zhou, "A visible light positioning system based on a particle filter and deep learning," *IEEE Transactions on Aerospace and Electronic Systems*, vol. 60, no. 3, pp. 2735–2748, 2024.

[20] Z. Zhu, Y. Yang, M. Chen, C. Guo, J. Cheng, and S. Cui, "A survey on indoor visible light positioning systems: Fundamentals, applications, and challenges," *IEEE Communications Surveys & Tutorials*, p. 1–1, 2024.

[21] M. F. Keskin, A. D. Sezer, and S. Gezici, "Localization via visible light systems," *Proceedings of the IEEE*, vol. 106, pp. 1063–1088, June 2018.

[22] H. Haas, L. Yin, C. Chen, S. Videv, D. Parol, E. Poves, H. Alshaer, and M. S. Islim, "Introduction to indoor networking concepts and challenges in LiFi," *Journal of Optical Communications and Networking*, vol. 12, p. A190, 12 2019.

[23] C. Jenila and R. Jeyachitra, "Green indoor optical wireless communication systems: Pathway towards pervasive deployment," *Digital Communications and Networks*, vol. 7, pp. 410–444, 9 2020.

[24] A. Boixader, C. Labella, M. Catalan, and J. Paradells, "A High-Accuracy, scalable and affordable indoor positioning system using visible light positioning for automated guided vehicles," *Electronics*, vol. 13, p. 82, 12 2023.

[25] R. Wang, G. Niu, Q. Cao, C. S. Chen, and S.-W. Ho, "A survey of Visible-Light-Communication-Based indoor Positioning Systems," *Sensors*, vol. 24, p. 5197, 8 2024.

[26] S. Bastiaens, M. Alijani, W. Joseph, and D. Plets, "Visible light positioning as a next-generation indoor positioning technology: A tutorial," *IEEE Communications Surveys & Tutorials*, vol. 26, no. 4, p. 2867–2913, 2024.

[27] A. Sahin, Y. S. Eroglu, I. Guvenc, N. Pala, and M. Yuksel, "Hybrid 3-D localization for visible light communication systems," *Journal of Lightwave Technology*, vol. 33, pp. 4589–4599, Nov. 2015.

[28] S.-H. Yang, H.-S. Kim, Y.-H. Son, and S.-K. Han, "Three-dimensional visible light indoor localization using AOA and RSS with multiple optical receivers," *Journal of Lightwave Technology*, vol. 32, pp. 2480–2485, July 2014.

[29] T.-H. Do, J. Hwang, and M. Yoo, "TDoA based indoor visible light positioning systems," in *2013 Fifth International Conference on Ubiquitous and Future Networks (ICUFN)*, pp. 456–458, 2013.

[30] H. Steendam, T. Q. Wang, and J. Armstrong, "Theoretical lower bound for indoor visible light positioning using received signal strength measurements and an aperture-based receiver," *Journal of Lightwave Technology*, vol. 35, pp. 309–319, Jan 2017.

[31] X. Zhang, J. Duan, Y. Fu, and A. Shi, "Theoretical accuracy analysis of indoor visible light communication positioning system based on received signal strength indicator," *Journal of Lightwave Technology*, vol. 32, no. 21, pp. 3578–3584, 2014.

[32] H. Steendam, T. Q. Wang, and J. Armstrong, "Cramer-Rao bound for indoor visible light positioning using an aperture-based angular-diversity receiver," in *2016 IEEE International Conference on Communications (ICC)*, pp. 1–6, May 2016.

[33] H. Steendam, T. Q. Wang, and J. Armstrong, "Cramer-Rao bound for AOA-based VLP with an aperture-based receiver," in *2017 IEEE International Conference on Communications (ICC)*, pp. 1–6, 2017.

[34] G. Kail, P. Maechler, N. Preyss, and A. Burg, "Robust asynchronous indoor localization using led lighting," in *2014 IEEE International Conference on Acoustics, Speech and Signal Processing (ICASSP)*, pp. 1866–1870, 2014.

[35] B. Zhou, A. Liu, and V. Lau, "On the fundamental performance limit of visible light-based positioning," in *13th International Conference on Signal Processing and Communication Systems (ICSPCS)*, pp. 1–6, 2019.

[36] I. Iddrisu and S. Gezici, "Visible light positioning under luminous flux degradation of LEDs," *IEEE Transactions on Aerospace and Electronic Systems*, vol. 61, no. 2, pp. 1648–1659, 2025.

[37] M. F. Keskin, S. Gezici, and O. Arikan, "Direct and two-step positioning in visible light systems," *IEEE Transactions on Communications*, vol. 66, pp. 239–254, Jan. 2018.

[38] S. Shen, S. Li, and H. Steendam, "Simultaneous position and orientation estimation for visible light systems with multiple LEDs and multiple PDs," *IEEE Journal on Selected Areas in Communications*, vol. 38, no. 8, pp. 1866–1879, 2020.

[39] Y. Chen, W. Guan, J. Li, and H. Song, "Indoor real-time 3-d visible light positioning system using fingerprinting and extreme learning machine," *IEEE Access*, vol. 8, pp. 13875–13886, 2020.

[40] F. Alam, M. T. Chew, T. Wenge, and G. S. Gupta, "An accurate visible light positioning system using regenerated fingerprint database based on calibrated propagation model," *IEEE Transactions on Instrumentation and Measurement*, vol. 68, no. 8, pp. 2714–2723, 2019.

[41] T. Yuan, Y. Xu, Y. Wang, P. Han, and J. Chen, "A tilt receiver correction method for visible light positioning using machine learning method," *IEEE Photonics Journal*, vol. 10, no. 6, pp. 1–12, 2018.

[42] M. Saadi, T. Ahmad, Y. Zhao, and L. Wuttisttikulkij, "An led based indoor localization system using k-means clustering," in *2016 15th IEEE International Conference on Machine Learning and Applications (ICMLA)*, pp. 246–252, 2016.

[43] A. Gradim, P. Fonseca, L. N. Alves, and R. E. Mohamed, "On the usage of machine learning techniques to improve position accuracy in visible light positioning systems," in *2018 11th International Symposium on Communication Systems, Networks & Digital Signal Processing (CSNDSP)*, pp. 1–6, 2018.

[44] X. Guo, S. Shao, N. Ansari, and A. Khreishah, "Indoor localization using visible light via fusion of multiple classifiers," *IEEE Photonics Journal*, vol. 9, no. 6, pp. 1–16, 2017.

[45] R. Liu, Z. Liang, K. Yang, and W. Li, "Machine learning based visible light indoor positioning with single-led and single rotatable photo detector," *IEEE Photonics Journal*, vol. 14, no. 3, pp. 1–11, 2022.

[46] A. H. A. Bakar, T. Glass, H. Y. Tee, F. Alam, and M. Legg, "Accurate visible light positioning using multiple-photodiode receiver and machine learning," *IEEE Transactions on Instrumentation and Measurement*, vol. 70, pp. 1–12, 2021.

[47] X. Li, Y. Cao, and C. Chen, "Machine learning based high accuracy indoor visible light location algorithm," in *2018 IEEE International Conference on Smart Internet of Things (SmartIoT)*, pp. 198–203, 2018.

[48] X. Cao, Y. Zhuang, G. Chen, X. Wang, X. Yang, and B. Zhou, "A visible light positioning system based on a particle filter and deep learning," *IEEE Transactions on Aerospace and Electronic Systems*, vol. 60, no. 3, pp. 2735–2748, 2024.

[49] M. Saadi, Z. Saeed, T. Ahmad, M. K. Saleem, and L. Wuttisittikulkij, "Visible light-based indoor localization using k-means clustering and linear regression," *Transactions on Emerging Telecommunications Technologies*, vol. 30, 02 2019.

[50] H. Huang, A. Yang, L. Feng, G. Ni, and a. Guo, "Artificial neural-network-based visible light positioning algorithm with a diffuse optical channel," *Chinese Optics Letters*, vol. 15, pp. 050601–50605, 05 2017.

[51] X. Guo, F. Hu, N. R. Elikplim, and L. Li, "Indoor localization using visible light via two-layer fusion network," *IEEE Access*, vol. 7, pp. 16421–16430, 2019.

[52] M. A. Arfaoui, M. D. Soltani, I. Tavakkolnia, A. Ghrayeb, C. M. Assi, M. Safari, and H. Haas, "Invoking deep learning for joint estimation of indoor lifi user position and orientation," *IEEE Journal on Selected Areas in Communications*, vol. 39, no. 9, pp. 2890–2905, 2021.

[53] B. Deng, F. Wang, L. Qin, and X. Hu, "A visible light 3d positioning system for underground mines based on convolutional neural network combining inception module and attention mechanism," *Photonics*, vol. 10, p. 918, 08 2023.

[54] H. Q. Tran and C. Ha, "High precision weighted optimum k-nearest neighbors algorithm for indoor visible light positioning applications," *IEEE Access*, vol. 8, pp. 114597–114607, 2020.

[55] M. Van, N. Tuan, T. The Son, H. Le Minh, and A. Burton, "Weighted k-nearest neighbor model for indoor vlc positioning," *IET Communications*, vol. 11, pp. 864 – 871, 05 2017.

[56] M. Xu, W. Xia, Z. Jia, Y. Zhu, and L. Shen, "A vlc-based 3-d indoor positioning system using fingerprinting and k-nearest neighbor," in *2017 IEEE 85th Vehicular Technology Conference (VTC Spring)*, pp. 1–5, 2017.

[57] H. Tran and C. Ha, "Machine learning in indoor visible light positioning systems: A review," *Neurocomputing*, vol. 491, 03 2022.

[58] O. Yazar and S. Gezici, "Optimal pulse design for visible light positioning systems," *Signal Processing*, vol. 191, p. 108334, Feb 2022.

[59] M. F. Keskin, A. D. Sezer, and S. Gezici, "Optimal and robust power allocation for visible light positioning systems under illumination constraints," *IEEE Transactions on Communications*, vol. 67, no. 1, pp. 527–542, 2019.

[60] S. Ma, R. Yang, B. Li, Y. Chen, H. Li, Y. Wu, M. Safari, S. Li, and N. Al-Dhahirxs, "Optimal power allocation for integrated visible light positioning and communication system with a single led-lamp," *IEEE Transactions on Communications*, vol. 70, p. 6734–6747, Oct 2022.

[61] S. Ma, R. Yang, C. Du, H. Li, Y. Wu, N. Al-Dhahir, and S. Li, "Robust power allocation for integrated visible light positioning and communication networks," *IEEE Transactions on Communications*, vol. 71, p. 4764–4777, Aug 2023.

[62] O. Yazar, M. F. Keskin, and S. Gezici, "Power-efficient positioning for visible light systems via chance constrained optimization," *IEEE Transactions on Aerospace and Electronic Systems*, vol. 56, p. 4124–4131, Oct 2020.

[63] S. Shi, G. Gui, Y. Lin, C. Yuen, O. A. Dobre, and F. Adachi, "Joint beamformer design and power allocation method for hybrid rf-vlcp system," *IEEE Internet of Things Journal*, vol. 11, p. 7878–7892, Mar 2024.

[64] A. Singh, A. Srivastava, V. A. Bohara, and A. K. Jagadeesan, "Optimal led power allocation framework for a location-assisted indoor visible light communication system," *IEEE Photonics Journal*, vol. 14, p. 1–14, Jun 2022.

[65] R. Yaz and S. Gezici, "Power allocation for LED arrays in asynchronous visible light positioning systems," 2025.

[66] F. Kokdogan and S. Gezici, "Intelligent reflecting surfaces for visible light positioning based on received power measurements," *IEEE Transactions on Vehicular Technology*, vol. 73, no. 9, pp. 13108–13121, 2024.

[67] S. D. Lausnay, L. D. Strycker, J. P. Goemaere, B. Nauwelaers, and N. Stevens, "A survey on multiple access visible light positioning," in *IEEE International Conference on Emerging Technologies and Innovative Business Practices for the Transformation of Societies (EmergiTech)*, pp. 38–42, Aug. 2016.

[68] D. Karunatilaka, F. Zafar, V. Kalavally, and R. Parthiban, "LED based indoor visible light communications: State of the art," *IEEE Communications Surveys & Tutorials*, vol. 17, no. 3, pp. 1649–1678, 2015.

[69] W. Zhang, M. I. S. Chowdhury, and M. Kavehrad, "Asynchronous indoor positioning system based on visible light communications," *Optical Engineering*, vol. 53, no. 4, pp. 1–9, 2014.

[70] M. F. Keskin and S. Gezici, "Comparative theoretical analysis of distance estimation in visible light positioning systems," *Journal of Lightwave Technology*, vol. 34, no. 3, pp. 854–865, 2016.

[71] T. Komine and M. Nakagawa, "Fundamental analysis for visible-light communication system using LED lights," *IEEE Transactions on Consumer Electronics*, vol. 50, pp. 100–107, Feb. 2004.

[72] E. Gonendik and S. Gezici, "Fundamental limits on RSS based range estimation in visible light positioning systems," *IEEE Communications Letters*, vol. 19, no. 12, pp. 2138–2141, 2015.

[73] J. M. Kahn and J. R. Barry, "Wireless infrared communications," *Proceedings of the IEEE*, vol. 85, pp. 265–298, Feb. 1997.

[74] A. M. Abdelhady, A. K. S. Salem, O. Amin, B. Shihada, and M.-S. Alouini, "Visible light communications via intelligent reflecting surfaces: Metasurfaces vs mirror arrays," *IEEE Open Journal of the Communications Society*, vol. 2, pp. 1–20, 2021.

[75] D. Gürgünoğlu, B. Dulek, and S. Gezici, "Power adaptation for vector parameter estimation according to Fisher information based optimality criteria," *Signal Processing*, vol. 192, p. 108390, 2022.

[76] H. V. Poor, *An Introduction to Signal Detection and Estimation*. New York: Springer-Verlag, 2 ed., 1994.

[77] M. Clerc, *Particle Swarm Optimization*. Wiley, 2006.

[78] S. Boyd and L. Vandenberghe, *Convex Optimization*. Cambridge University Press, 2004.

[79] K. B. Petersen and M. S. Pedersen, "The matrix cookbook," 2008.

[80] A. Gad, "Particle swarm optimization algorithm and its applications: A systematic review," *Archives of Computational Methods in Engineering*, vol. 29, p. 2531–2561, 04 2022.

[81] Y. S. Eroglu, A. Sahin, I. Guvenc, N. Pala, and M. Yuksel, "Multi-element transmitter design and performance evaluation for visible light communication," in *2015 IEEE Globecom Workshops*, pp. 1–6, Dec. 2015.

[82] A. Mostafa and L. Lampe, "Optimal and robust beamforming for secure transmission in MISO visible-light communication links," *IEEE Transactions on Signal Processing*, vol. 64, pp. 6501–6516, Dec. 2016.